A Pandas complex adapted for piRNA-guided transposon silencing

Kang Zhao[#1], Sha Cheng[#2], Na Miao[#1], Ping Xu[#1,3], Xiaohua Lu[#1], Ming Wang[1], Yuhan Zhang[2], Xun Yuan[2], Weiwei Liu[1], Xin Lu[1], Xuan Ouyang[1], Peng Zhou[1], Jiaqi Gu[1,4], Yiqun Zhang[1], Ding Qiu[1], Shan Wang[1], Zhaohui Jin[2], Youzhong Wan[3], Jinbiao Ma[4], Hong Cheng[2], Ying Huang[2,5], Yang Yu[1,5]

[1]Institute of Biophysics, Key Laboratory of RNA Biology, Chinese Academy of Sciences, University of Chinese Academy of Sciences, Beijing, China, 100101
[2]State Key Laboratory of Molecular Biology, Shanghai Key Laboratory of Molecular Andrology, CAS Center for Excellence in Molecular Cell Science, Shanghai Institute of Biochemistry and Cell Biology, Chinese Academy of Sciences, University of Chinese Academy of Sciences, Shanghai, China, 200031
[3]School of Life Sciences, National Engineering Laboratory of AIDS Vaccine, Key Laboratory for Molecular Enzymology and Engineering of Ministry of Education, Jilin University, Changchun, Jilin, China, 130012
[4]State Key Laboratory of Genetic Engineering, Department of Biochemistry, School of Life Sciences, Fudan University, Shanghai, China, 200438

[#]contributed equally

[5]correspondence: yuyang@ibp.ac.cn; huangy@sibcb.ac.cn

Keywords: piRNA, transposon silencing, dNxf2, Panoramix, crystal structure, *Drosophila*, dNxf1/TAP, dNxt1/p15

Abstract

The repression of transposons by the Piwi-interacting RNA (piRNA) pathway is essential to protect animal germ cells. In *Drosophila* ovaries, Panoramix (Panx) enforces transcriptional silencing by binding to the target-engaged Piwi-piRNA complex, although the precise mechanisms by which this occur remain elusive. Here, we show that Panx functions together with a germline specific paralogue of a nuclear export factor, dNxf2, and its cofactor dNxt1 (p15) as a ternary complex to suppress transposon expression. Structural and functional analysis demonstrate that dNxf2 binds Panx via its UBA domain and play an important role in transposon silencing through binding to transposon transcripts directly. Unexpectedly, dNxf2 interacts directly with dNxf1 (TAP), which is also essential for transposon silencing. Transient tethering of dNxf2 to nascent transcripts leads to their nuclear retention. Therefore, we propose that dNxf2 may function as a Pandas (Panoramix-dNxf2 dependent TAP/p15 silencing) complex, which counteracts the canonical RNA exporting machinery (TAP/p15) and restricts transposons to nuclear peripheries. Our findings may have broader implications for understanding how RNA metabolism modulates epigenetic gene silencing and heterochromatin formation.

57 Transposons are highly abundant in eukaryotes, which make up nearly half of human genome. To
58 maintain eukaryotic genome integrity, nascent transcripts of transposons are often targeted by
59 nuclear Argonaute proteins for transcriptional gene silencing (TGS)[1-5]. In animal gonads, the PIWI-
60 clade Argonautes guided by piRNAs (PIWI-interacting RNA) are thought to recognize nascent
61 transposon transcripts and direct sequence-specific heterochromatin formation[3]. As a critical
62 cofactor of *Drosophila* nuclear Piwi, Panoramix (Panx, also known as Silencio) links the target-
63 engaged Piwi-piRNA complex to the general silencing machinery[6,7]. Enforced tethering of Panx to
64 nascent transcripts leads to cotranscriptional silencing and correlates with deposition of histone H3
65 lysine 9 trimethylation (H3K9me3) marks[6,7]. However, the mechanism by which Panx mediates the
66 repression remains unknown. An equally important question is why H3K9me3 marks are not always
67 sufficient for transposon silencing[8].
68
69 To understand this fundamental question, we cross-examined proteins that co-
70 immunoprecipitated with Panx (Extended Data Fig. 1a) with piRNA pathway candidate genes from
71 RNA interference (RNAi) screens[9-12]. Unexpectedly, dNxf2 was identified as a potential cofactor of
72 Panx (Extended Data Fig.1a-c). dNxf2 belongs to an evolutionarily conserved NXF (nuclear export
73 factor) family of proteins, yet depletion of dNxf2 had no effect on polyadenylated mRNA export[13,14].
74 Instead, dNxf2 and its cofactor dNxt1 (also known as p15) were both identified in two published
75 RNAi screens as being essential for transposon silencing[9,10]. Similar to Panx, dNxf2 is specifically
76 expressed in female gonads (Extended Data Fig.1d).
77
78 To validate the interaction between Panx and dNxf2, GFP immunoprecipitation from ovaries
79 expressing GFP-Panx fusion under its native promoter was performed. Results of mass
80 spectrometry analysis (Extended Data Fig. 1b) and western blotting demonstrated that endogenous
81 dNxf2 is associated with Panx (Fig. 1a). Likewise, Halo-tagged dNxf2 was able to precipitate

82 endogenous Panx from Ovarian Somatic Cell (OSC) lysates with a Halo-tag integrated into the C-
83 terminus of Nxf2 (Fig. 1b and Extended Data Fig. 6e). We next tested if dNxf2 is functionally
84 required for Panx-mediated silencing. The luciferase transcripts with BoxB sites in their 3′
85 untranslated regions are repressed if λN-Panx is tethered[6,7]. The expression level of luciferase was
86 measured upon germline-specific knockdowns of either dNxf2 or dNxt1 (Fig. 1c). Despite
87 constitutive tethering of λN-Panx, loss of either dNxf2 or dNxt1 significantly weakened the ability of
88 Panx to repress the reporter, as compared to the controls (Zuc or attp2, Fig. 1c). Consistent with
89 the reporter de-repression, transposon transcripts are elevated upon dNxf2 RNAi (Extended Data
90 Fig. 1e). Taken together, our data suggested that dNxf2 and dNxt1 may function as a heterodimer
91 either with or downstream of Panx to suppress transposon expression.
92
93 Next, we used RNA sequencing (RNA-seq) to examine global effects on transposon
94 expression with germline-specific knockdowns of dNxf2, compared with Panx RNAi (Fig. 1d-f). As
95 expected, dNxf2 knockdown triggered a dramatic increase of transposon transcripts (Fig. 1d),
96 similar to that of Panx (Fig. 1e-f), suggesting that dNxf2 is specifically required for silencing of
97 transposons repressed by Panx. To rule out off-target effects of RNAi, mutants of dNxf2 were
98 generated using CRISPR/Cas9 technique (Extended Data Fig. 2a)[15]. The dNxf2 mutant female
99 flies were completely sterile with a deletion of 20 amino acids at the N-terminus of dNxf2 (Extended
100 Data Fig. 2b), similar to other core piRNA pathway mutants[6]. Loss of dNxf2 showed little effect on
101 Piwi nuclear localization or stability (Extended Data Fig.2c-d), indicating that dNxf2 functions as an
102 effector protein. Furthermore, dNxf2 mutants showed global up-regulation of transposons
103 (Extended Data Fig. 2e-g) and de-repression of the luciferase reporter despite λN-Panx tethering
104 (Extended Data Fig. 3a). The protein level of endogenous Panx is noticeably reduced in the
105 absence of dNxf2 (Extended Data Fig. 2d). To rule out the possibility that dNxf2 might affect
106 transposons indirectly via Panx stability, transposon expression levels were measured upon

107 overexpression of λN-Flag-Panx under the dNxf2 mutant background (Extended Data Fig. 3a-e).
108 Still, dNxf2 mutant female flies lost transposon control (Extended Data Fig. 3c-d) and were
109 completely sterile as if Panx did not exist (Extended Data Fig. 3e).
110
111 The striking phenotypic similarities between dNxf2 and Panx prompted us to test whether these
112 two proteins interact directly. We used yeast two-hybrid (Y2H) assays to determine the interacting
113 regions. The domain architecture of dNxf2 is very similar to that of the canonical RNA export factor,
114 dNxf1/TAP (also known as sbr, Fig. 2a). Both proteins contain leucine-rich repeats (LRR), an RNA
115 recognition motif (RRM), a nuclear transport factor 2 (NTF2)-like domain, and a ubiquitin-
116 associated domain (UBA). Y2H assays were performed to examine the interactions. Interestingly,
117 Panx only interacts with the UBA domain of dNxf2 but not that of dNxf1 (Fig. 2b), indicating that
118 this interaction between Panx and dNxf2 is specific (Fig. 2b). Surprisingly, neither full length nor
119 the NTF2+UBA fragment of dNxf2 could bind Panx (Fig. 2b), suggesting that the UBA domain of
120 dNxf2 might be in a "closed" conformation in the presence of the NTF2 domain. In this regard, the
121 interactions between dNxt1 and the NTF2 domains of either dNxf2 or dNxf1 are also weakened in
122 the presence of its UBA domain (Fig. 2c). Since *Drosophila* Nxt1 itself is absent in the Y2H system,
123 we tested whether dNxt1 might release the UBA domain from the NTF2 domain to permit Panx
124 binding. Indeed, ectopic expression of dNxt1 is sufficient to allow full length dNxf2 to interact with
125 Panx in a Y2H assay (Fig. 2d). Next, we mapped the minimum region of Panx down to residues
126 315-343 (NIR, d<u>N</u>xf2 <u>i</u>nteracting <u>r</u>egion) as sufficient for UBA binding (Fig. 2e and Extended Data
127 Fig. 3f). Consistent with the fact that dNxt1 forms a heterodimer with dNxf2[13], we found that dNxt1
128 co-migrates with a fusion protein of dNxf2$^{NTF2+UBA}$-(Gly-Ser)$_4$-Panx^{NIR} by size-exclusion
129 chromatography (Fig. 2f), suggesting that Panx, dNxf2, and dNxt1 may exist as a ternary complex.
130 We were not able to crystalize the dNxf2^{NTF2} domain, instead, we crystallized dNxf1^{NTF2} in complex
131 with dNxt1 and determined the structure (Extended Data Fig. 4a). Residues that may involve in the

132 binding of dNxf2^{NTF2} to dNxt1 were modeled according to the sequence alignment result and the
133 structure of dNxf1^{NTF2} (Extended Data Fig. 4a). dNxf2^{NTF2} maintained most, if not all, residues that
134 interact with dNxt1 as validated by the Y2H and co-immunoprecipitation assays (Extended Data
135 Fig. 4a-e), indicating that the interaction mode of dNxf2^{NTF2} and dNxt1 complex is similar to that of
136 dNxf1^{NTF2} and dNxt1.
137
138 Purified Panx^{NIR} forms a stable complex with the UBA domain of dNxf2 with a dissociation
139 constant of ~3.2 μM as measured by isothermal titration calorimetry (ITC) (Fig. 2g). To further
140 explore the molecular basis of interactions between dNxf2 and Panx, the crystal structure of the
141 dNxf2-Panx complex was determined (Fig. 3a-d). Despite many efforts, only the fusion protein of
142 dNxf2^{UBA}-(Gly-Ser)$_4$-Panx^{NIR} could be successfully crystallized. The structure was solved to a 1.5
143 Å resolution (Table S1). dNxf2^{UBA} forms a compact three-helix bundle (α1–α3) with a 3_{10}-helix (η1)
144 at the C-terminus (Fig. 3b). The Panx^{NIR} is folded into a long α-helix and lays on the hydrophobic
145 surface formed by α2 and α3 (Fig. 3b-c and Extended Data Fig. 4f). A324, A328, V331, L332, and
146 I335 on Panx interact with V800, F819, F826, F840, L823 and I827 on dNxf2 via hydrophobic
147 interactions (Fig. 3d). Moreover, R321 and R327 on Panx form salt bridges with D837 and E799
148 on Nxf2^{UBA}, respectively (Fig. 3d). To validate the intermolecular interactions between dNxf2 and
149 Panx, key residues on the interacting interface were mutated (Fig. 3e). While either L823A or
150 D837A single point mutation affected the binding between Panx and dNxf2^{UBA}, the double point
151 mutation of dNxf2^{UBA} (F826A/I827A) nearly abolished its interaction with Panx in both Y2H and co-
152 immunoprecipitation assays (Fig. 3e-f), highlighting the significant contribution of these residues in
153 Panx binding.
154
155 In contrast to the highly charged surface of the Nxf1-type UBA (i.e. hsNxf1 or scMex67),
156 dNxf2^{UBA} favors hydrophobic binding with Panx (Fig. 3c and Extended Data Fig. 5a-b). Key residues

157 on the interacting interface are highly conserved among different *Drosophila* species but altered in
158 the Nxf1-type UBA (Extended Data Fig. 5a). On the opposite surface of the Nxf1-type UBA, a
159 hydrophobic pocket is formed to accommodate the FxFG peptide of the nuclear pore complex (NPC)
160 (Extended Data Fig. 5c-d). However, this pocket is missing in dNxf2^{UBA} due to a salt bridge formed
161 between K829 and E814 (Extended Data Fig. 5c). Additionally, the bulky side chain of L825 on
162 dNxf2^{UBA} may hinder FG binding (Extended Data Fig. 5c). In contrast, the corresponding amino
163 acids in hsNxf1 (A602) or scMex67 (G583) contain much smaller side chains (Extended Data Fig.
164 5c-d), therefore, give space for FxFG interactions. Consistent with the structural prediction,
165 dNxf2^{UBA} failed to interact with the FG-repeats of Nup214, a NPC component known to interact with
166 dNxf1^{UBA} (Extended Data Fig. 5e)[14]. Since two copies of FG binding domains (NTF2 and UBA) are
167 minimally required for proper RNA export[16], dNxf2 lacks at least one copy of the FG binding domain
168 (UBA) and thus cannot export RNAs.
169
170 To validate the importance of the direct interactions between dNxf2 and Panx *in vivo*, a
171 previously described λN/BoxB luciferase reporter system was used to check if artificial tethering of
172 dNxf2 could lead to repression. As expected, significant repression upon tethering of a λN-dNxf2
173 fusion protein (Fig. 3g) was observed, unlike that of the negative controls (λN-YFP or GFP-dNxf2
174 lacking a λN-tag). Similar to Panx, the level of λN-dNxf2 mediated repression was in a dosage-
175 dependent manner, which is correlated with the number of BoxB binding sites (Fig. 3h). Most
176 importantly, the repression is dependent on the presence of the dNxf2 UBA domain (Fig. 3g, dNxf2-
177 ΔUBA).
178
179 The domain architecture of dNxf2 is similar to Nxf1 proteins which also contains RNA binding
180 domains at the N-terminus, implying that dNxf2 might directly bind to transposon transcripts *in vivo*
181 (Fig. 3a)[13]. To validate this hypothesis, we performed GoldCLIP/RT-qPCR experiments, which

182 reply on a covalent attachment of the Halo-tag to its ligand on beads, affording a denaturing
183 purification of crosslinked protein-RNA complexes[17]. A Halo-tag was inserted to the C-terminus of
184 dNxf2 (dNxf2-Halo) using CRISPR/Cas9 (Extended Data Fig. 6a-f)[18]. Strikingly, following UV
185 crosslinking, transposon transcripts (mdg1), but not rp49, remained attached to the dNxf2-Halo
186 fusion protein despite denaturing washes (Extended Data Fig. 6b-c). The association is dependent
187 on UV crosslinking, demonstrating a direct binding between mdg1 and dNxf2 (Extended Data Fig.
188 6b-c). Interestingly, the interaction was only observed when both histone H1 and Heterochromatin
189 Protein 1a (HP1a) were depleted by RNAi, but not in the control knockdown (Extended Data Fig.
190 6b-c), supporting that the majority of transposon transcripts remain suppressed in a wildtype
191 background. Low steady-state levels of transposon nascent RNAs make it extremely difficult to
192 obtain reasonable signals in an already inefficient UV crosslinking experiment. Nevertheless, upon
193 removal of the downstream silencing factors (H1 and HP1a), transposon transcripts accumulate
194 and bind to dNxf2 (Extended Data Fig. 6b). In contrast, Frogger didn't show any detectable CLIP
195 signal despite of the dramatic up-regulation of its transcripts upon H1 and HP1a double RNAi
196 (Extended Data Fig. 6d). This result suggests that the binding of dNxf2 to transposon is likely
197 piRNA-guided, since Frogger is not targeted by Piwi-piRNAs in OSCs[19]. In order to obtain enough
198 material, we performed GoldCLIP-seq experiments using dNxf2-Halo knock-in OSCs depleted of
199 Maelstrom, a piRNA pathway effector component either parallel or downstream of H3K9me3
200 establishment on transposons (personal communications with Mikiko Siomi)[8]. Consistent with the
201 RT-qPCR results, CLIP-seq demonstrated that dNxf2 preferentially binds to Piwi-targeted
202 transposons (Fig. 4a and Extended Data Fig. 7). Moreover, the RNA binding domains (RBD) of
203 dNxf2 are essential for silencing in the tethering assays (Extended Data Fig. 8). Therefore,
204 $dNxf2^{RBD}$ are likely to be involved in the effector step of silencing rather than the Piwi-dependent
205 recruitment of dNxf2. Collectively, our data strongly argues that Panx and dNxf2/dNxt1 function
206 together as a stable complex to directly suppress transposons that are targeted by Piwi-piRNAs.

207

208 Loss of Panx leads to significantly decreased H3K9me3 marks over transposons[6,7]. We next
209 tested whether removing dNxf2 could result in a similar phenomenon. Since Panx is unstable in
210 the absence of dNxf2 (Extended Data Fig. 2d), we performed H3K9me3 ChIP-qPCR assays over
211 several transposons as well as the Firefly-10xBoxB reporter tethered with λN-Flag-Panx. H3K9me3
212 showed rather mild changes upon removal of dNxf2. This is in direct contrast to the dramatic
213 upregulation of transposon transcripts in the absence of dNxf2 (Extended Data Fig. 3c-d and 9).
214 This result suggested that transposon silencing and H3K9me3 deposition are uncoupled in *dNxf2*
215 mutants. Interestingly, we found that Het-A chromatin left nuclear peripheries upon loss of either
216 Panx or dNxf2 (Extended Data Fig. 10)[20]. Transposon transcripts (I element) which are targeted by
217 piRNAs have been previously shown to accumulate within nucleus[21]. Thus, we proposed that
218 certain RNA export machineries might be modulated by the piRNA pathway to prevent transposon
219 transcripts from getting translated. Human Nxf1/TAP has been reported to dimerize with most NXF
220 family members to regulate RNA export[22,23]. We wondered whether dNxf2 might interact with dNxf1
221 *in vivo*. GFP-tagged dNxf2 can co-immunoprecipitate Halo-tagged dNxf1 from OSC lysates (Fig.
222 4b). Either NTF2 or UBA domain of dNxf1 is sufficient to interact with $dNxf2^{NTF2}$ (Fig. 4c and
223 Extended Data Fig. 11). Most importantly, GST pull-down assays demonstrated a direct binding
224 between dNxf1 and dNxf2 (Fig. 4d and Extended Data Fig. 12). Consistent with the involvement of
225 dNxf1 in transposon silencing, dNxf1 was found in a genome-wide RNAi screen for piRNA pathway
226 components[11]. Female flies with mutant alleles of dNxf1 are sterile and have defects in meiotic
227 spindles[24], a phenotype reminiscent of core piRNA pathway mutants[25,26]. Therefore, we tested if
228 dNxf1 is required for Panx-mediated silencing. Indeed, germline specific depletion of dNxf1
229 significantly impaired the repression of the reporter mediated by tethering λN-Panx, thereby
230 genetically placing dNxf1 at the effector step of transcriptional silencing (Fig. 4e). To rule out any
231 indirect or off-target effects of dNxf1 knockdowns, we introduced either wild-type dNxf1 or a

232 truncated version missing the RNA binding domains (ΔRBD=RRM+LRR) as transgenic flies. As
233 expected, wild-type dNxf1 suppressed the transposon overexpression caused by the shRNA
234 targeting the 5' untranslated region of endogenous dNxf1 (Fig. 4f). Importantly, the truncated dNxf1
235 lacking the RNA cargo binding domains (ΔRBD) maintained the ability to rescue transposon
236 silencing (Fig. 4f). Since the RBD of dNxf1 is required for RNA export[16], our results strongly suggest
237 a specialized involvement of dNxf1 in transposon silencing. Next, we sought to directly visualize
238 potential changes in RNA localization by using a rapamycin-inducible tethering system (Fig. 4g and
239 Extended Data Fig. 13). GFP mRNAs containing 10x copies of BoxB binding sites tethered with
240 λN-FKBP are mostly localized in the cytoplasm (Fig. 4g and Movie S5-12). Upon Rapamycin
241 treatment, λN-FKBP dimerizes with FRB-dNxf2 fusion protein, allowing tethering of dNxf2 to the
242 GFP mRNAs. Intriguingly, GFP mRNAs start to accumulate at nuclear peripheries upon binding of
243 FRB-dNxf2 (Fig. 4g). The effect is specific to dNxf2 since FRB alone failed to cause any change.
244 Given this, we named this multi-protein complex as Pandas (Panx-dNxf2 dependent TAP/p15
245 silencing). Our data raise the possibility that deterring the function of dNxf1 in transposon RNA
246 export may be a key intermediate event in piRNA-guided silencing (Extended Data Fig. 14). In the
247 absence of dNxf2, Panx failed to efficiently suppress either transposons or the tethered reporters,
248 despite the overexpression of λN-Flag-Panx (Extended Data Fig. 3a-e). In this regard, λN-Flag-
249 Panx was unable to stay bound to the de-repressed transposon chromatin as measured by Flag
250 ChIP-qPCR (Extended Data Fig. 13c). Similarly, the Flag-ChIP signals over the tethered reporter
251 were also diminished even when λN-Flag-Panx was constitutively tethered to the nascent RNAs.
252 This is consistent with the observation that direct tethering of HP1a to nascent RNAs via λN/BoxB
253 system failed to install silencing[7]. This is in stark contrast to HP1a's ability to induce
254 heterochromatin formation if tethered via DNA[27-30]. Our data provided a possible explanation why
255 RNA tethering of HP1a could not induce silencing. Therefore, sequestering nascent transposon
256 transcripts within nucleus might be important to fully establish heterochromatin and enforce

257 silencing. We believed that, by removing dNxf2, we had uncovered an intermediate state of
258 silencing during heterochromatin formation.
259
260 Like any coding mRNA, if not restrained by Piwi-piRNAs, transposon transcripts would likewise
261 be transported into the cytoplasm by the dNxf1/dNxt1 exporting machinery[14,21]. In piRNA-guided
262 TGS, dNxf2/dNxt1 may function together with Panx as a stable complex to counteract this process
263 (Extended Data Fig. 13). Our structure provided mechanistic insights into why dNxf2^{UBA} prefers to
264 bind the silencing factor Panx rather than the FG repeats of NPCs (Extended Data Fig. 5).
265 Accordingly, part of dNxf2's silencing function may be hijacking the RNA export machinery and
266 repurposing dNxf1 into a "dead-end" complex, hence trapping transposon transcripts within the
267 nucleus (Fig. 4g and Extended Data Fig. 12). Dam-ID showed that both Piwi and NPCs contacts
268 chromatin at the same regions[31]. In this regard, dNxf1 can localize to nuclear peripheries in which
269 most constitutive heterochromatin resides[13,32-34]. The mechanism of how dNxf2 prevents dNxf1
270 from exporting transposon transcripts requires further investigation. The fact that dimerization of
271 hsNxf1/TAP is important for RNA export raised a possibility that dNxf2 might block dNxf1-mediated
272 RNA export by preventing its dimerization[22,23]. Nevertheless, our data indicated that sequestering
273 transposons to nuclear peripheries via the Pandas complex may help to establish/maintain their
274 heterochromatic state (Extended Data Fig. 10 and Movie 1-4)[33,34]. Interestingly, recent evidence
275 demonstrated that hsNxf1 is required for efficient elongation of RNA polymerase II[35]. It is tempting
276 to speculate that the Pandas complex might also inhibit transcriptional elongation of transposons
277 via neutralizing dNxf1. In summary, we uncovered an unexpected role of transposon RNA export
278 blockage prior to transcriptional gene silencing. Our results will have broader implications for how
279 RNA metabolism modulates epigenetic gene silencing and heterochromatin formation (Extended
280 Data Fig. 14).
281

REFERENCES

1. Ge, D. T. & Zamore, P. D. Small RNA-directed silencing: the fly finds its inner fission yeast? *Curr. Biol.* **23,** R318–20 (2013).
2. Martienssen, R. & Moazed, D. RNAi and heterochromatin assembly. *Cold Spring Harb Perspect Biol* **7,** a019323 (2015).
3. Czech, B. & Hannon, G. J. One Loop to Rule Them All: The Ping-Pong Cycle and piRNA-Guided Silencing. *Trends Biochem. Sci.* **0,** (2016).
4. Ozata, D. M., Gainetdinov, I., Zoch, A., Carroll, D. X. N. O. X. & Zamore, P. D. PIWI-interacting RNAs: small RNAs with big functions. *Nat. Rev. Genet.* 1–20 (2018). doi:10.1038/s41576-018-0073-3
5. Gainetdinov, I., Colpan, C., Arif, A., Cecchini, K. & Zamore, P. D. A Single Mechanism of Biogenesis, Initiated and Directed by PIWI Proteins, Explains piRNA Production in Most Animals. *Mol. Cell* **71,** 775–790.e5 (2018).
6. Yu, Y. *et al.* Panoramix enforces piRNA-dependent cotranscriptional silencing. *Science* **350,** 339–342 (2015).
7. Sienski, G. *et al.* Silencio/CG9754 connects the Piwi-piRNA complex to the cellular heterochromatin machinery. *Genes Dev.* **29,** 2258–2271 (2015).
8. Sienski, G., Dönertas, D. & Brennecke, J. Transcriptional silencing of transposons by Piwi and maelstrom and its impact on chromatin state and gene expression. *Cell* **151,** 964–980 (2012).
9. Czech, B., Preall, J. B., McGinn, J. & Hannon, G. J. A transcriptome-wide RNAi screen in the Drosophila ovary reveals factors of the germline piRNA pathway. *Mol. Cell* **50,** 749–761 (2013).
10. Muerdter, F. *et al.* A genome-wide RNAi screen draws a genetic framework for transposon control and primary piRNA biogenesis in Drosophila. *Mol. Cell* **50,** 736–748 (2013).
11. Handler, D. *et al.* The genetic makeup of the Drosophila piRNA pathway. *Mol. Cell* **50,** 762–777 (2013).
12. Guruharsha, K. G. *et al.* A protein complex network of Drosophila melanogaster. *Cell* **147,** 690–703 (2011).
13. Herold, A., Klymenko, T. & Izaurralde, E. NXF1/p15 heterodimers are essential for mRNA nuclear export in Drosophila. *RNA* **7,** 1768–1780 (2001).
14. Katahira, J. Nuclear export of messenger RNA. *Genes (Basel)* **6,** 163–184 (2015).
15. Port, F., Chen, H.-M., Lee, T. & Bullock, S. L. Optimized CRISPR/Cas tools for efficient germline and somatic genome engineering in Drosophila. *Proc. Natl. Acad. Sci. U.S.A.* **111,** E2967–76 (2014).
16. Braun, I. C., Herold, A., Rode, M. & Izaurralde, E. Nuclear export of mRNA by TAP/NXF1 requires two nucleoporin-binding sites but not p15. *Mol. Cell. Biol.* **22,** 5405–5418 (2002).
17. Gu, J. *et al.* GoldCLIP: Gel-omitted Ligation-dependent CLIP. *Genomics Proteomics Bioinformatics* **16,** 136–143 (2018).
18. Savic, D. *et al.* CETCh-seq: CRISPR epitope tagging ChIP-seq of DNA-binding proteins. *Genome Res.* **25,** 1581–1589 (2015).
19. Iwasaki, Y. W. *et al.* Piwi Modulates Chromatin Accessibility by Regulating Multiple Factors Including Histone H1 to Repress Transposons. *Mol. Cell* **63,** 408–419 (2016).
20. Radion, E. *et al.* Key role of piRNAs in telomeric chromatin maintenance and telomere nuclear positioning in Drosophila germline. *Epigenetics Chromatin* **11,** 40 (2018).
21. Chambeyron, S. *et al.* piRNA-mediated nuclear accumulation of retrotransposon transcripts in the Drosophila female germline. *Proc. Natl. Acad. Sci. U.S.A.* **105,** 14964–14969 (2008).
22. Matzat, L. H., Berberoglu, S. & Lévesque, L. Formation of a Tap/NXF1 homotypic complex is mediated through the amino-terminal domain of Tap and enhances interaction with

332 nucleoporins. *Mol. Biol. Cell* **19,** 327–338 (2008).
333 23. Aibara, S., Katahira, J., Valkov, E. & Stewart, M. The principal mRNA nuclear export factor
334 NXF1:NXT1 forms a symmetric binding platform that facilitates export of retroviral CTE-
335 RNA. *Nucleic Acids Res.* **43,** 1883–1893 (2015).
336 24. Golubkova, E. V. *et al.* Dm nxf1/sbr gene affects the formation of meiotic spindle in female
337 Drosophila melanogaster. *Chromosome Res.* **17,** 833–845 (2009).
338 25. Czech, B. & Hannon, G. J. A Happy 3' Ending to the piRNA Maturation Story. *Cell* **164,**
339 838–840 (2016).
340 26. Khurana, J. S. & Theurkauf, W. piRNAs, transposon silencing, and Drosophila germline
341 development. *J. Cell Biol.* **191,** 905–913 (2010).
342 27. Danzer, J. R. & Wallrath, L. L. Mechanisms of HP1-mediated gene silencing in Drosophila.
343 *Development* **131,** 3571–3580 (2004).
344 28. Hines, K. A. *et al.* Domains of heterochromatin protein 1 required for Drosophila
345 melanogaster heterochromatin spreading. *Genetics* **182,** 967–977 (2009).
346 29. Li, Y., Danzer, J. R., Alvarez, P., Belmont, A. S. & Wallrath, L. L. Effects of tethering HP1 to
347 euchromatic regions of the Drosophila genome. *Development* **130,** 1817–1824 (2003).
348 30. Azzaz, A. M. *et al.* Human heterochromatin protein 1α promotes nucleosome associations
349 that drive chromatin condensation. *J. Biol. Chem.* **289,** 6850–6861 (2014).
350 31. Ilyin, A. A. *et al.* Piwi interacts with chromatin at nuclear pores and promiscuously binds
351 nuclear transcripts in Drosophila ovarian somatic cells. *Nucleic Acids Res.* **45,** 7666–7680
352 (2017).
353 32. Kerkow, D. E. *et al.* The structure of the NXF2/NXT1 heterodimeric complex reveals the
354 combined specificity and versatility of the NTF2-like fold. *J. Mol. Biol.* **415,** 649–665 (2012).
355 33. van Steensel, B. & Belmont, A. S. Lamina-Associated Domains: Links with Chromosome
356 Architecture, Heterochromatin, and Gene Repression. *Cell* **169,** 780–791 (2017).
357 34. Towbin, B. D., Meister, P. & Gasser, S. M. The nuclear envelope--a scaffold for silencing?
358 *Curr. Opin. Genet. Dev.* **19,** 180–186 (2009).
359 35. Chen, S. *et al.* The mRNA Export Receptor NXF1 Coordinates Transcriptional Dynamics,
360 Alternative Polyadenylation, and mRNA Export. *Mol. Cell* **74,** 118–131.e7 (2019).
361

362 **ACKNOWLEDGEMENTS**

363 We thank Shanghai Science Research Center for their instrumental support and technical
364 assistance. We thank the staff from BL19U1 beamline at Shanghai Synchrotron Radiation Facility
365 (SSRF) for assistance during data collection. We thank Ms. Shuoguo Li from Center for Biological
366 Imaging (CBI), Institute of Biophysics, Chinese Academy of Science for her help of taking and
367 analyzing SIM images. This work was supported in part by grants from the Ministry of Science and
368 Technology of China (2017YFA0504200 to Y.Y.) and by grants from the National Natural Science
369 Foundation of China (91640102 and 31870741 to Y.H.; 91640105 and 31770875 to Y.Y.), and the
370 Chinese Academy of Sciences Facility-based Open Research Program and the State Key
371 Laboratory of Molecular Biology.

372

373 **AUTHOR CONTRIBUTIONS**

374 Y.Y. and Y.H. conceived the project and wrote the manuscript. K.Z. constructed the dNxf2-
375 Halo knock-in OSCs and established the dNxf2 mutant. K.Z., P.X., W.W.L. and X.H.L.
376 performed co-immunoprecipitations, tethering assays, transgenic fly constructions, RNA-
377 seq, RT-qPCR experiments. S.C. and X.Y. performed structural studies, beta-gal activity
378 assays, and ITC experiments; K.Z., Z.J., F.Q., P.Z., S.W., X.O., J.Q.G. and P.X. performed
379 cloning. S.C. and X.L. performed Y2H assays. K.Z. and X.O. performed FACS analysis.
380 N.M. preformed FISH and RNAi experiments. M.W. and Y.Z. performed bioinformatics
381 analysis. Y.Z.W., J.M. and H.C. provided critical reagents and advice; All authors
382 discussed the results and commented on the manuscript.

383

384 **COMPETING INTERESTS**

385 The authors declare that there is no conflict of interests.

386

387 **MATERIALS & CORRESPONDENCE**

388 All materials and correspondence requesta should be addressed to yuyang@ibp.ac.cn.

389

Figure 1

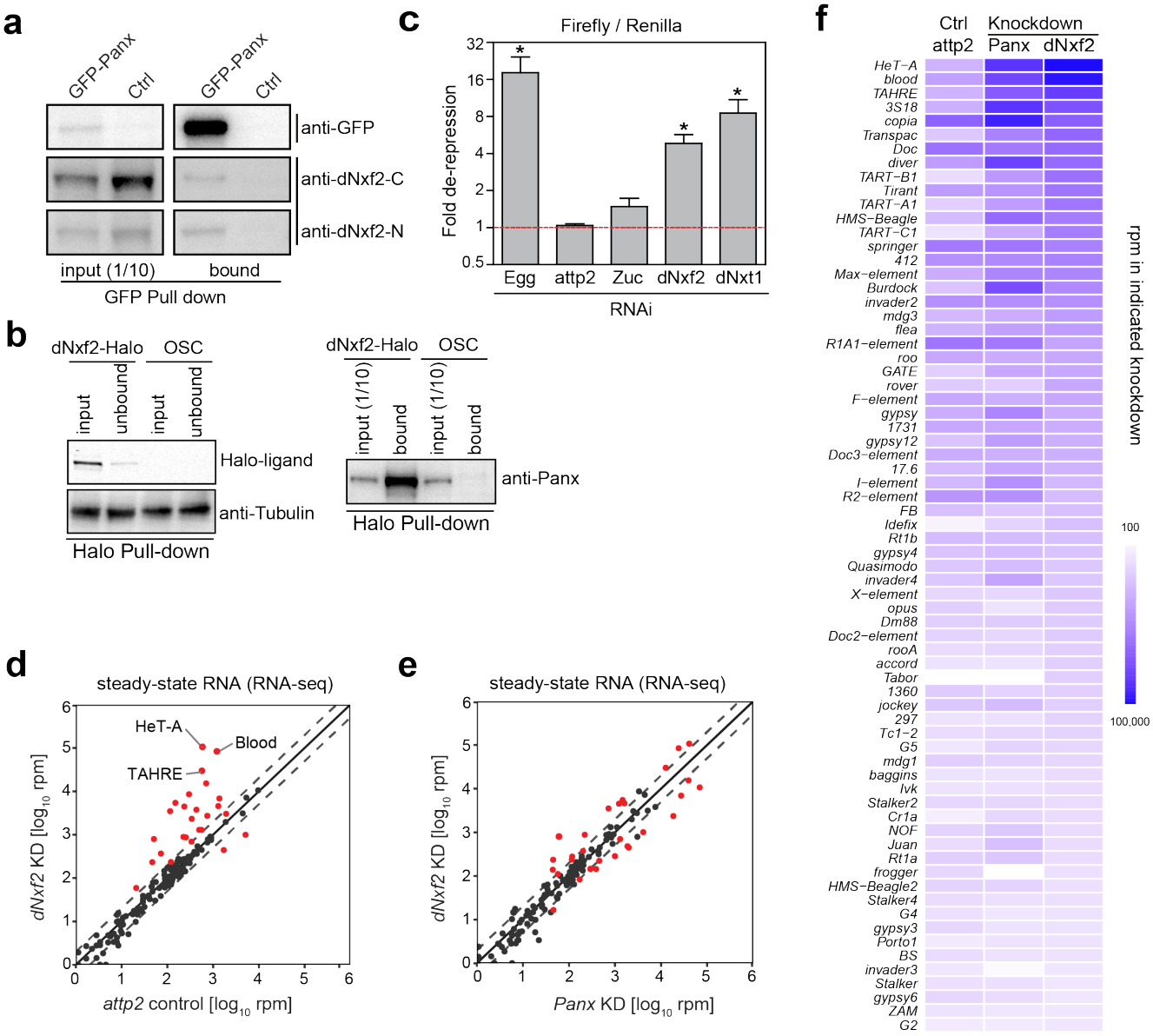
a
GFP-Panx
Ctrl
GFP-Panx
Ctrl
anti-GFP
anti-dNxf2-C
anti-dNxf2-N
input (1/10)
bound
GFP Pull down
b
dNxf2-Halo
OSC
input
unbound
input
unbound
Halo-ligand
anti-Tubulin
Halo Pull-down
dNxf2-Halo
OSC
input (1/10)
bound
input (1/10)
bound
anti-Panx
Halo Pull-down
c
Firefly / Renilla
Fold de-repression
Egg
attp2
Zuc
dNxf2
dNxt1
RNAi
d
steady-state RNA (RNA-seq)
HeT-A
Blood
TAHRE
dNxf2 KD [log10 rpm]
attp2 control [log10 rpm]
e
steady-state RNA (RNA-seq)
dNxf2 KD [log10 rpm]
Panx KD [log10 rpm]
f
Ctrl
Knockdown
attp2
Panx
dNxf2
HeT-A
blood
TAHRE
3S18
copia
Transpac
Doc
diver
TART-B1
Tirant
TART-A1
HMS-Beagle
TART-C1
springer
412
Max-element
Burdock
invader2
mdg3
flea
R1A1-element
roo
GATE
rover
F-element
gypsy
1731
gypsy12
Doc3-element
17.6
I-element
R2-element
FB
Idefix
Rt1b
gypsy4
Quasimodo
invader4
X-element
opus
Dm88
Doc2-element
rooA
accord
Tabor
1360
jockey
297
Tc1-2
G5
mdg1
baggins
Ivk
Stalker2
Cr1a
NOF
Juan
Rt1a
frogger
HMS-Beagle2
Stalker4
G4
gypsy3
Porto1
BS
invader3
Stalker
gypsy6
ZAM
G2
rpm in indicated knockdown
100
100,000

390 **Figure 1. dNxf2 functions as a cofactor of Panx in the piRNA pathway.**

391 **a**, Western blots showing co-immunoprecipitation of endogenous dNxf2 with GFP-Panx from ovary
392 lysates. Two different rabbit polyclonal monospecific dNxf2 (dNxf2-N and dNxf2-C) antibodies were
393 used to detect endogenous dNxf2. **b**, Halo-ligand staining and western blots showing co-
394 immunoprecipitation of endogenous Panx with dNxf2-Halo driven by the endogenous dNxf2
395 promoter from OSC lysates. A rabbit polyclonal monospecific Panx antibody was used to detect
396 endogenous Panx. Left panel shows depletion of dNxf2-Halo proteins in the unbound sample by
397 Halo beads, and the anti-Tubulin blots serve as loading controls; Right panel shows endogenous
398 Panx proteins. **c**, The effects of germline (*nanos*-GAL4) knockdown of the indicated genes on
399 Renilla-normalized Firefly luciferase activity of the reporter while tethering λN-Panx. For
400 comparison, the relative value of the attp2 control was used for normalization. Data show
401 mean ± s.d. (n = 15; *P = 1.41387E-07). **d**, Comparison of steady-state RNA levels are shown as
402 reads per million (rpm) mapping to the sense strand of each transposon consensus from the *nanos*-
403 GAL4 driven knockdown for dNxf2 (Y axis) versus control (X axis). Dashed lines indicate two-fold
404 changes. The average of two replicates is shown. KD = knockdown. Red dots indicate transposon
405 elements with significant changes. **e**, Comparison of steady-state RNA levels (RNA-seq; shown as
406 RPM) mapping to the sense strands of each transposon consensus from the *nanos*-GAL4 driven
407 knockdowns of the indicated genes. Red dots indicate transposon elements with significant
408 changes from **d**. **f**, Heat map displaying steady-state RNA levels (RNA-seq) as reads per million
409 (rpm) for top 70 detected transposons from the *nanos*-GAL4 driven knockdowns of the indicated
410 genes in a blue-white scale.

411

Figure 2

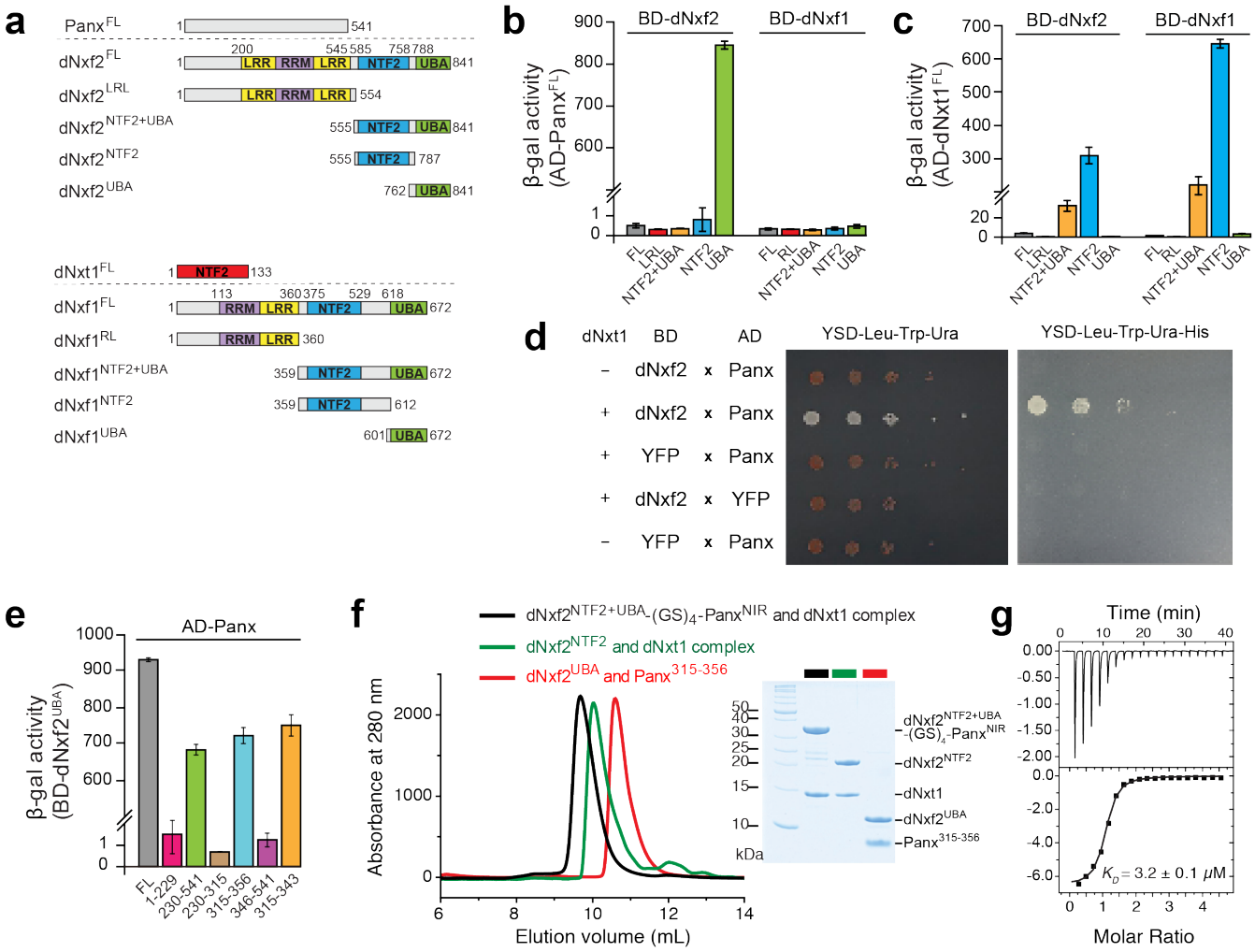
a
Panx^FL
dNxf2^FL
dNxf2^LRL
dNxf2^NTF2+UBA
dNxf2^NTF2
dNxf2^UBA
LRR
RRM
NTF2
UBA
dNxt1^FL
dNxf1^FL
dNxf1^RL
dNxf1^NTF2+UBA
dNxf1^NTF2
dNxf1^UBA
b
BD-dNxf2
BD-dNxf1
β-gal activity (AD-Panx^FL)
c
β-gal activity (AD-dNxt1^FL)
d
dNxt1
BD
AD
YSD-Leu-Trp-Ura
YSD-Leu-Trp-Ura-His
e
AD-Panx
β-gal activity (BD-dNxf2^UBA)
f
dNxf2^NTF2+UBA-(GS)4-Panx^NIR and dNxt1 complex
dNxf2^NTF2 and dNxt1 complex
dNxf2^UBA and Panx^315-356
Absorbance at 280 nm
Elution volume (mL)
kDa
dNxf2^NTF2+UBA-(GS)4-Panx^NIR
dNxf2^NTF2
dNxt1
dNxf2^UBA
Panx^315-356
g
Time (min)
Molar Ratio
K_D = 3.2 ± 0.1 μM

412 **Figure 2. The UBA domain of dNxf2 interacts with Panx directly.**

413 **a**, Domain architectures of Panx, dNxf2, dNxf1, and dNxt1 are shown. Numbers above the
414 diagrams correspond to amino acid residues of each protein. Domain names are abbreviated within
415 respective colored region. **b-e**, Y2H assays mapping the interacting regions between *Drosophila*
416 Nxf1/2 and Panx or dNxt1. Interactions were determined by either measuring the beta-
417 galactosidase activity produced by the reporter gene or growth on YSD media lacking the indicated
418 essential amino acid or Uracil. Data are averages of three independent experiments (n=3). Proteins
419 or fragments shown above the dashed line are used as preys in the assays. **b**, Y2H assays mapping
420 regions of *Drosophila* Nxf1/2 that interact with Panx. **c**, Y2H assays mapping regions of *Drosophila*
421 Nxf1/2 that interact with dNxt. **d**, Yeast three hybrid determining the requirement of dNxt1 for
422 Nxf2:Panx interaction. **e**, Y2H assays mapping minimum regions of Panx that interact with $dNxf2^{UBA}$.
423 **f**, Left panel shows the size exclusive chromatography profile of the NTF2 and UBA domains of
424 dNxf2 forming heterodimers with dNxt1 and $Panx^{NIR}$ in solution, respectively. A dNxf2 fragment
425 spanning the NTF2 and UBA domains that is covalently linked to $Panx^{NIR}$ forms a stable complex
426 with dNxt1. Right panel, SDS-PAGE shows the components of the peak in the elution profile. Color
427 schemes used for the three complexes are indicated in the key. **g**, Quantification of the dissociation
428 constant for the interaction between $dNxf2^{UBA}$ and $Panx^{NIR}$ as measured by an isothermal titration
429 calorimetry assay.

430

431

432

433

434

435

436

Figure 3

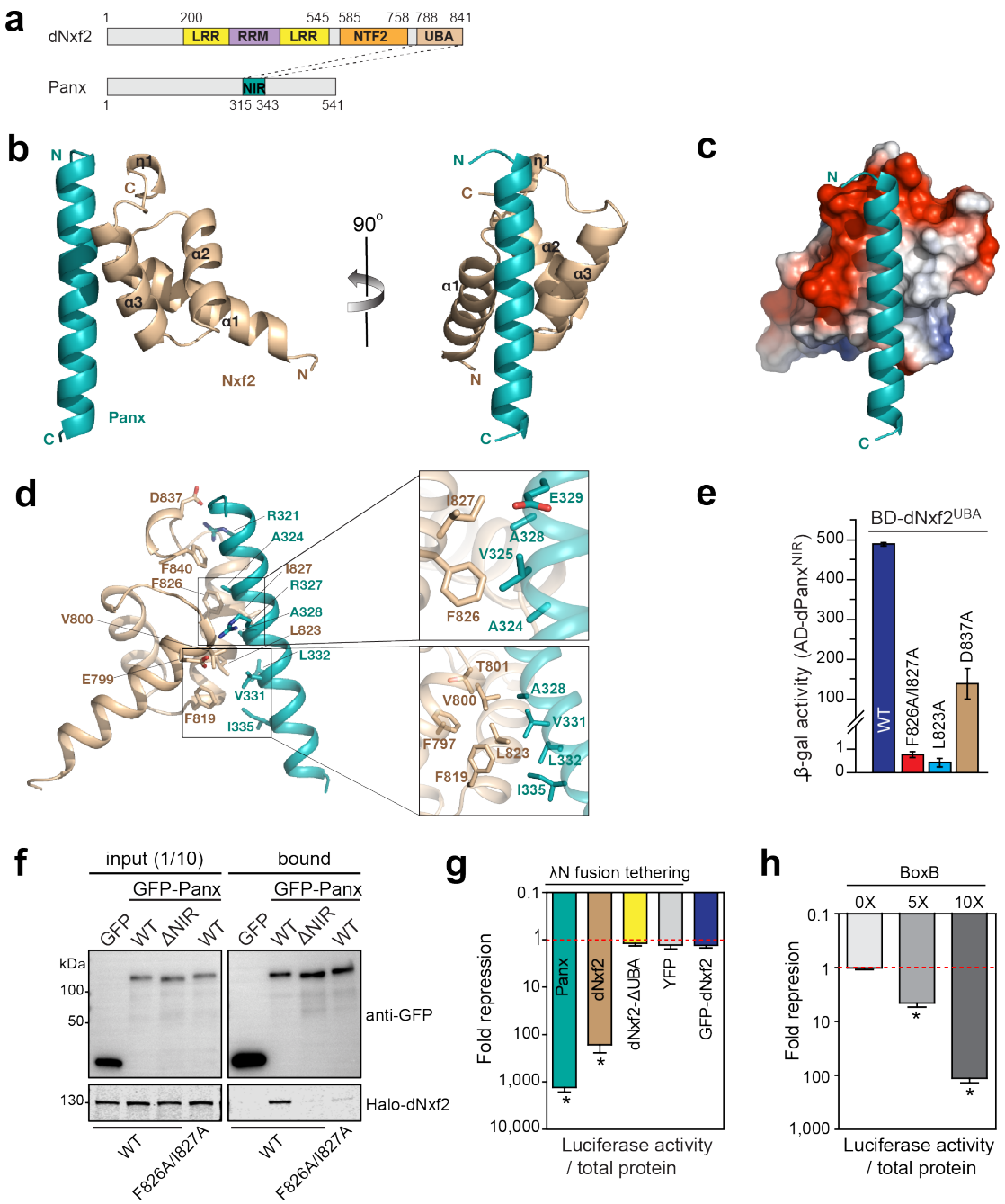
a
dNxf2
1
200
545
585
758
788
841
LRR
RRM
LRR
NTF2
UBA
Panx
NIR
1
315
343
541
b
N
η1
C
α2
α3
α1
Nxf2
N
Panx
C
90°
N
η1
C
α2
α3
α1
N
C
c
N
C
d
D837
R321
A324
F840
F826
I827
R327
A328
L823
V800
L332
E799
V331
F819
I335
I827
E329
A328
V325
F826
A324
T801
A328
V800
V331
F797
L823
L332
F819
I335
e
BD-dNxf2UBA
β-gal activity (AD-dPanxNIR)
500
400
300
200
100
1
0
WT
F826A/I827A
L823A
D837A
f
input (1/10)
bound
GFP-Panx
GFP-Panx
GFP
WT
ΔNIR
WT
GFP
WT
ΔNIR
WT
kDa
100
50
anti-GFP
130
Halo-dNxf2
WT
F826A/I827A
WT
F826A/I827A
g
λN fusion tethering
Fold repression
0.1
1
10
100
1,000
10,000
Panx
dNxf2
dNxf2-ΔUBA
YFP
GFP-dNxf2
Luciferase activity
/ total protein
h
BoxB
0X
5X
10X
Fold repression
0.1
1
10
100
1,000
Luciferase activity
/ total protein

437 **Figure 3. Structure of dNxf2^{UBA} in complex with Panx^{NIR}.**

438 **a**, Schematic of interacting region between dNxf2 and Panx. Numbers above or below the diagrams
439 correspond to amino acid residues of dNxf2 or Panx, respectively. Domain names are abbreviated
440 within respective colored region. NIR, dNxf2 interacting region. **b**, Left, cartoon representation of
441 dNxf2^{UBA} in complex with Panx^{NIR}. The dNxf2^{UBA} and Panx^{NIR} fragment are colored in wheat and
442 teal, respectively. Right, a view rotated 90° around the vertical axis. **c**, Electrostatic potential
443 analysis showing the Panx-binding surface of dNxf2^{UBA}. Panx^{NIR} is shown in cartoon mode. **d**, A
444 detailed view showing the interactions between dNxf2^{UBA} and Panx^{NIR}. Key residues involved in
445 binding are shown in sticks. Close-up views of hydrophobic interactions between dNxf2^{UBA} and
446 Panx^{NIR} are shown on the right. **e**, Y2H assays measuring the binding of wild-type or mutant
447 dNxf2^{UBA} with Panx^{NIR}. Mutations of key residues are indicated along the bars. **f**, Western blots and
448 Halo-ligand staining showing co-immunoprecipitation of GFP-tagged Panx or its NIR deletion
449 mutant (ΔNIR) with Halo-tagged dNxf2 or its F826A/I827A double mutant from OSC cells. GFP
450 serves as a negative control. **g**, Effects of the indicated λN fusion proteins or a non-tethering control
451 (GFP-dNxf2) on luciferase activity of the reporters integrated into the attP2 landing site. Data show
452 mean ± s.d. (n = 15; *P = 1.41387E-07). **h**, The effects of λN-dNxf2 tethering on luciferase activity
453 of reporters with increasing number of BoxB sites. All reporters are integrated into the same
454 genomic locus (attP2 landing site). Fold repression is calculated as total protein-normalized Firefly
455 luciferase luminescent values of the control (no tethering) divided by that of the indicated
456 experiments. Data show mean ± s.d. (n = 15; *P = 1.41387E-07).

457

458

Figure 4

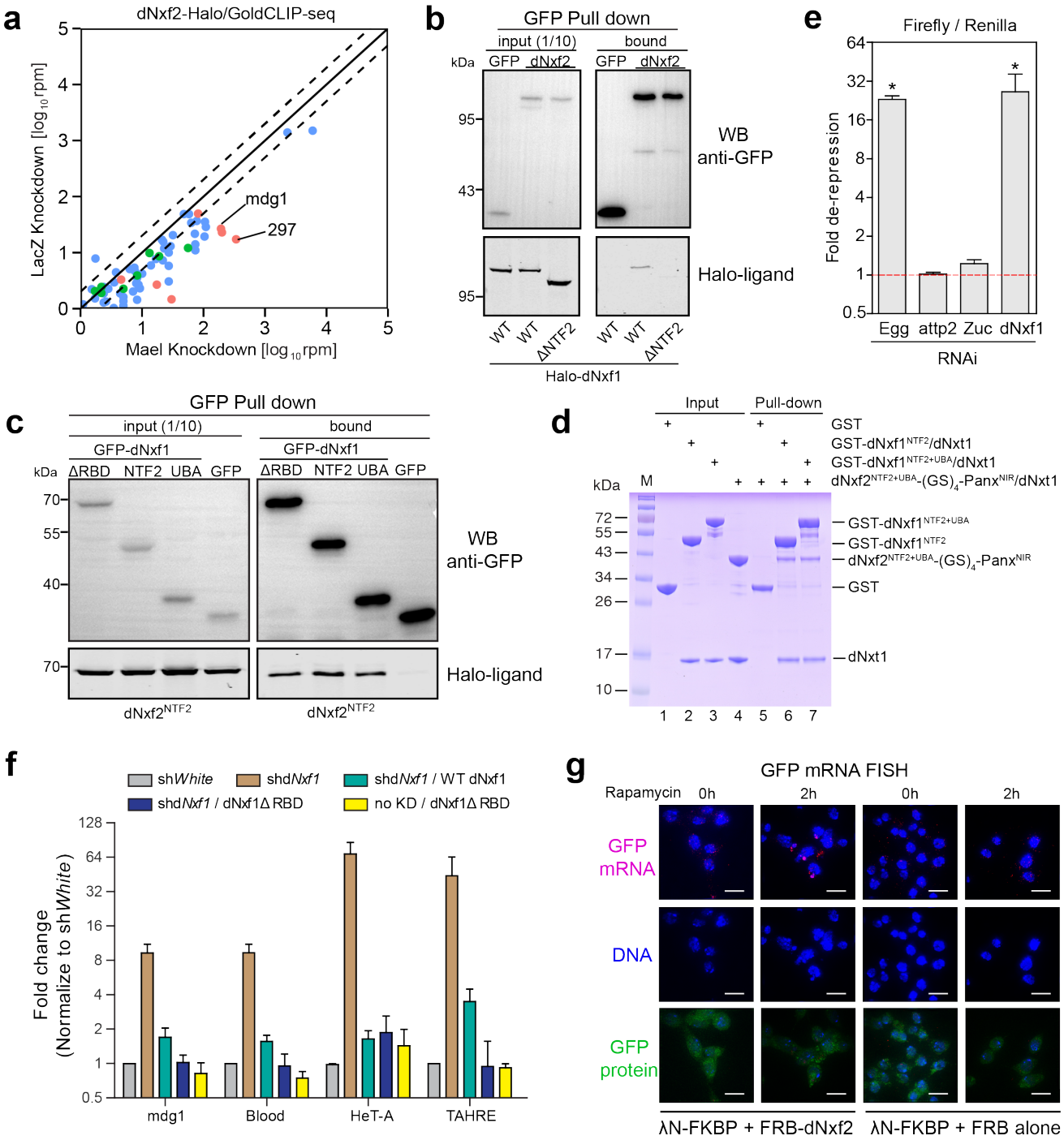
a
dNxf2-Halo/GoldCLIP-seq
LacZ Knockdown [log10rpm]
Mael Knockdown [log10rpm]
mdg1
297
b
GFP Pull down
input (1/10)
bound
kDa
GFP
dNxf2
WB anti-GFP
Halo-ligand
WT
ΔNTF2
Halo-dNxf1
e
Firefly / Renilla
Fold de-repression
Egg
attp2
Zuc
dNxf1
RNAi
c
GFP Pull down
input (1/10)
bound
GFP-dNxf1
ΔRBD
NTF2
UBA
GFP
WB anti-GFP
Halo-ligand
dNxf2NTF2
d
Input
Pull-down
GST
GST-dNxf1NTF2/dNxt1
GST-dNxf1NTF2+UBA/dNxt1
dNxf2NTF2+UBA-(GS)4-PanxNIR/dNxt1
kDa
M
GST-dNxf1NTF2+UBA
GST-dNxf1NTF2
dNxf2NTF2+UBA-(GS)4-PanxNIR
GST
dNxt1
f
shWhite
shdNxf1
shdNxf1 / WT dNxf1
shdNxf1 / dNxf1ΔRBD
no KD / dNxf1ΔRBD
Fold change (Normalize to shWhite)
mdg1
Blood
HeT-A
TAHRE
g
GFP mRNA FISH
Rapamycin
0h
2h
GFP mRNA
DNA
GFP protein
λN-FKBP + FRB-dNxf2
λN-FKBP + FRB alone

459 **Figure 4. The Pandas complex is required for piRNA-guided transposon silencing.**

460 **a**, Comparison of GoldCLIP-seq are shown as reads per million (rpm) mapping to the sense strand
461 of each transposon consensus for Maelstrom (*X* axis) versus a LacZ control knockdown (*Y* axis).
462 A mammalian spike-in was used to normalize different samples. Dashed lines indicate two-fold
463 changes. The pooled reads from two replicates are shown. Red dots indicate Piwi-targeted
464 transposons, blue dots indicate H1-dependent transposons and green dots indicate other
465 transposons. **b**, Western blots and Halo-ligand staining showing co-immunoprecipitation of GFP-
466 tagged dNxf2 with Halo-tagged dNxf1 from OSC cells. ΔNTF2, Halo-dNxf1 lacking the NTF2
467 domain, and GFP serves as a negative control. **c**, Western blots and Halo-ligand staining showing
468 co-immunoprecipitation of Halo-tagged dNxf2-NTF2 domain with different domain truncations of
469 GFP-tagged dNxf1 from OSC cells. ΔRBD, dNxf1 lacking the N-terminus RRM and LRR domains;
470 GFP serves as a negative control. **d**, SDS-PAGE showing pulldown results of the $Nxf2^{NTF2+UBA}$-
471 (GS)4-$Panx^{NIR}$/dNxt1 complex by either GST-tagged dNxf1-NTF2 or dNxf1-(NTF2+UBA)
472 respectively, compared to a GST control. **e**, The effects of germline specific knockdown (nanos-
473 GAL4) of the indicated genes on Renilla-normalized Firefly luciferase activity of the reporter while
474 tethering λN-Panx. For comparison, the results from Fig. 1C (Egg, attp2 and Zuc) were shown here
475 again. Data show mean ± s.d. (n = 15; *P = 1.41387E-07). **f**, RT-qPCR results showing the effects
476 of germline (*nanos*-GAL4) knockdown of the indicated genes in the presence or absence of
477 different transgenes. Fold changes are calculated as rp49-normalized RNA levels divided by that
478 of the corresponding controls. Mean values ± s.d. from 3 independent experiments are shown. **g**,
479 SIM super-resolution microscopy of RNA FISH. Data showing the comparison of the localizations
480 of the reporter mRNAs tethered with λN-FKBP, upon transient recruitment of either FRB-dNxf2 or
481 FRB alone when treated with rapamycin for 2 hours to induce FKBP:FRB dimerization. DMSO
482 serves as a control. Top panel, RNA signal (red) with DAPI staining; middle, DAPI staining (blue);
483 bottom, RanGAP-GFP fusion protein (green) were shown. The scale bars represent 5 μM in length.

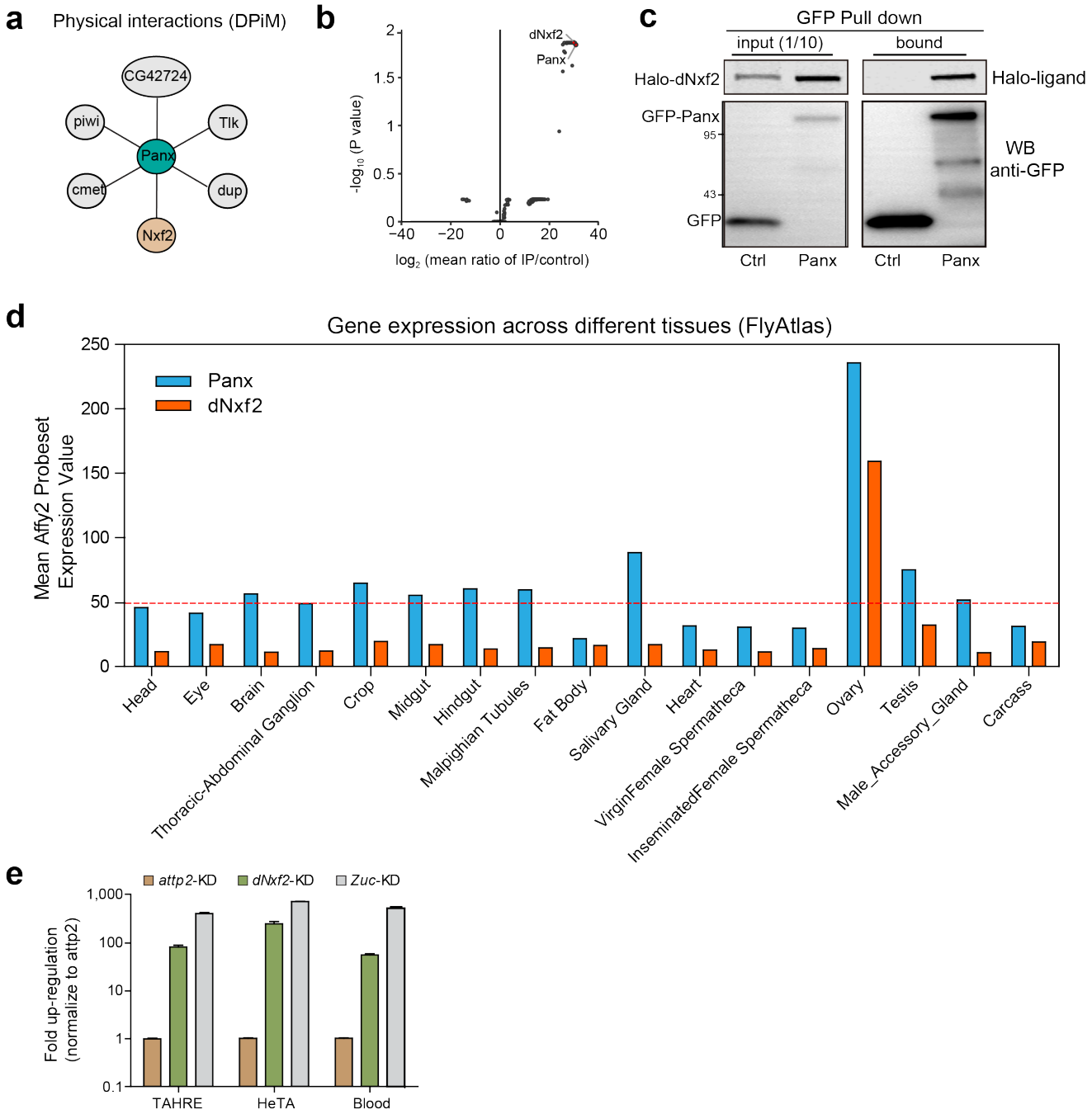

Extended Data Figure 1. dNxf2 binds to Panx and is required for transposon silencing. a, A network graph showing proteins co-immunoprecipitated with Flag-tagged Panx from the DPiM data downloaded from flybase.org. **b,** Volcano plots showing significance and enrichment values for proteins co-purified with GFP-Panx (n=2) from ovary lysates (the two most significantly enriched proteins are labeled). **c,** Western blots and Halo-ligand staining showing co-immunoprecipitation of GFP-tagged Panx with Halo-tagged dNxf2 from OSC cell lysates. GFP serves as a negative control. **d,** The expression profiles (*Y*-axis) of Panx and dNxf2 across different adult tissues (*X*-axis) are shown (red, Panx; blue, dNxf2). The mean affy2 probeset expression value (*X*-axis) is based on FlyAtlas anatomical microarray data downloaded from flybase.org. **e,** RT-qPCR results showing relative steady-state RNA levels of the indicated transposons for the germline specific (nanos-GAL4) knockdown of the indicated genes. The attp2 is used as a control**.** Fold changes are calculated as *rp49*-normalized RNA levels divided by that of the corresponding controls. Mean values ± s.d. from 3 independent experiments are shown.

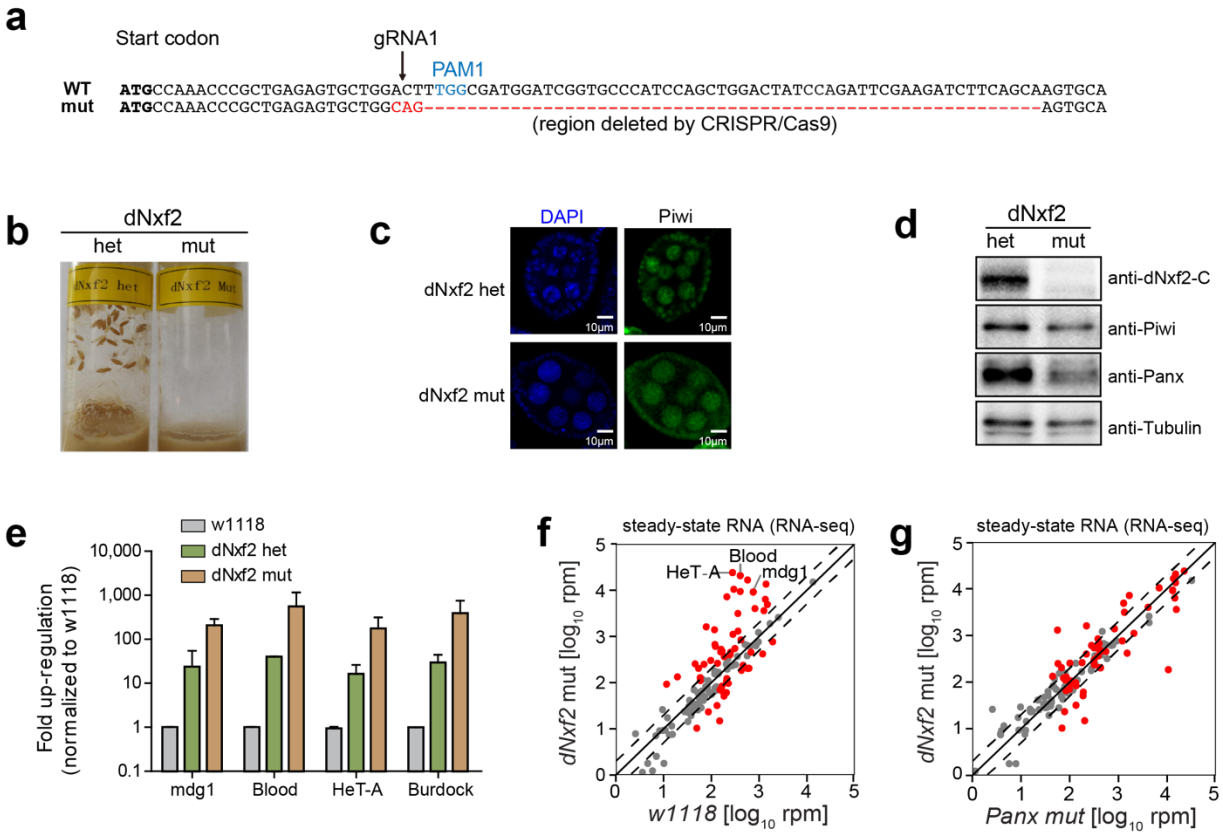

Extended Data Figure 2. dNxf2 mutant resembles Panx mutant. a, A schematic of CRISPR/Cas9-induced mutation in the open reading frame of dNxf2 is shown. Arrowheads indicate the cleavage sites targeted by the gRNA with the corresponding PAM site highlighted in light blue. The resulting mutant is shown below the wild-type sequence with the mutated/deleted region shown in red. **b,** Vials showing pupae from equal number of either heterozygous or mutant dNxf2 female flies crossed with OregonR males. **c,** Representative immunostaining of endogenous Piwi protein (green) from stage 5 ovaries of either heterozygous or mutant dNxf2. DAPI staining (blue) was used to indicate nuclei. **d,** Western blots showing protein expression level of endogenous dNxf2, Panx and Piwi from either heterozygous or mutant dNxf2 ovary lysates. Beta-tubulin serves as a loading control. **e,** RT-qPCR results showing relative steady-state RNA levels of the indicated transposons for the mutant or heterozygous dNxf2 ovaries, compared to the wildtype control (w1118). Fold changes are calculated as *rp49*-normalized RNA levels divided by that of the corresponding controls. Mean values ± s.d. from 3 independent experiments are shown. **f,** Comparison of steady-state RNA levels are shown as reads per million (rpm) mapping to the sense strands of each transposon consensus from dNxf2 mutant versus w1118 wild-type fly ovaries. Dashed lines indicate two-fold changes. The average of two replicates is shown. Red dots indicate transposon elements with significant changes. **g,** Comparison of steady-state RNA levels (RNA-seq; shown as RPM) mapping to the sense strands of each transposon consensus from dNxf2 mutant versus Panx mutant fly ovaries. Red dots indicate transposon elements with significant changes from **f**.

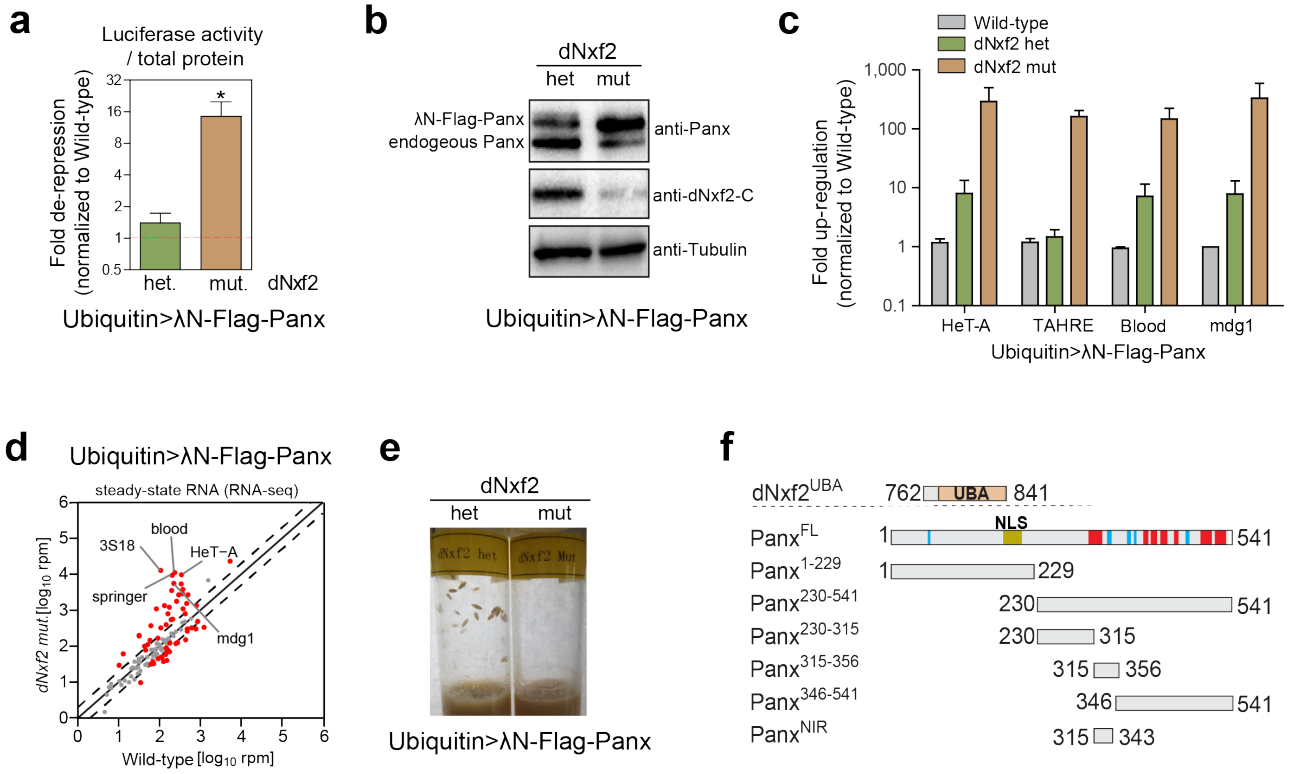

Extended Data Figure 3. dNxf2 is required for Panx-mediated transposon silencing. a, The expression of the total protein-normalized Firefly luciferase activity of the reporter under the indicated background (heterozygous control or transheterozygous mutant) while overexpressing λN-Flag-Panx driven by a Ubiquitin promoter. Data show mean ± s.d. (n = 15; *P = 1.41387E-07). **b,** Western blots showing protein expression level of endogenous dNxf2, Panx from either heterozygous or mutant dNxf2 ovary lysates while overexpressing λN-Flag-Panx driven by a Ubiquitin promoter. Beta-tubulin serves as a loading control. **c,** RT-qPCR results showing relative steady-state RNA levels of the indicated transposons for the mutant or heterozygous dNxf2 ovaries, compared to the wildtype control while overexpressing λN-Flag-Panx driven a Ubiquitin promoter. Fold changes are calculated as *rp49*-normalized RNA levels divided by that of the corresponding controls. Mean values ± s.d. from 3 independent experiments are shown. **d,** Comparison of steady-state RNA levels are shown as reads per million (rpm) mapping to the sense strands of each transposon consensus from dNxf2 mutant versus wild-type fly ovaries when overexpressing ubiquitin driven Panx. Dashed lines indicate two-fold changes. The average of two replicates is shown. Red dots indicate transposon elements with significant changes. **e,** Vials showing pupae from equal number of either heterozygous or mutant dNxf2 female flies when overexpressing ubiquitin driven Panx, mated with OregonR males. **f,** Schematic of full-length Panx and its truncated fragments used in the Y2H assays in Fig. 2e. Numbers corresponding to amino acid residues at either the N- or C-terminus of each protein fragment**.**

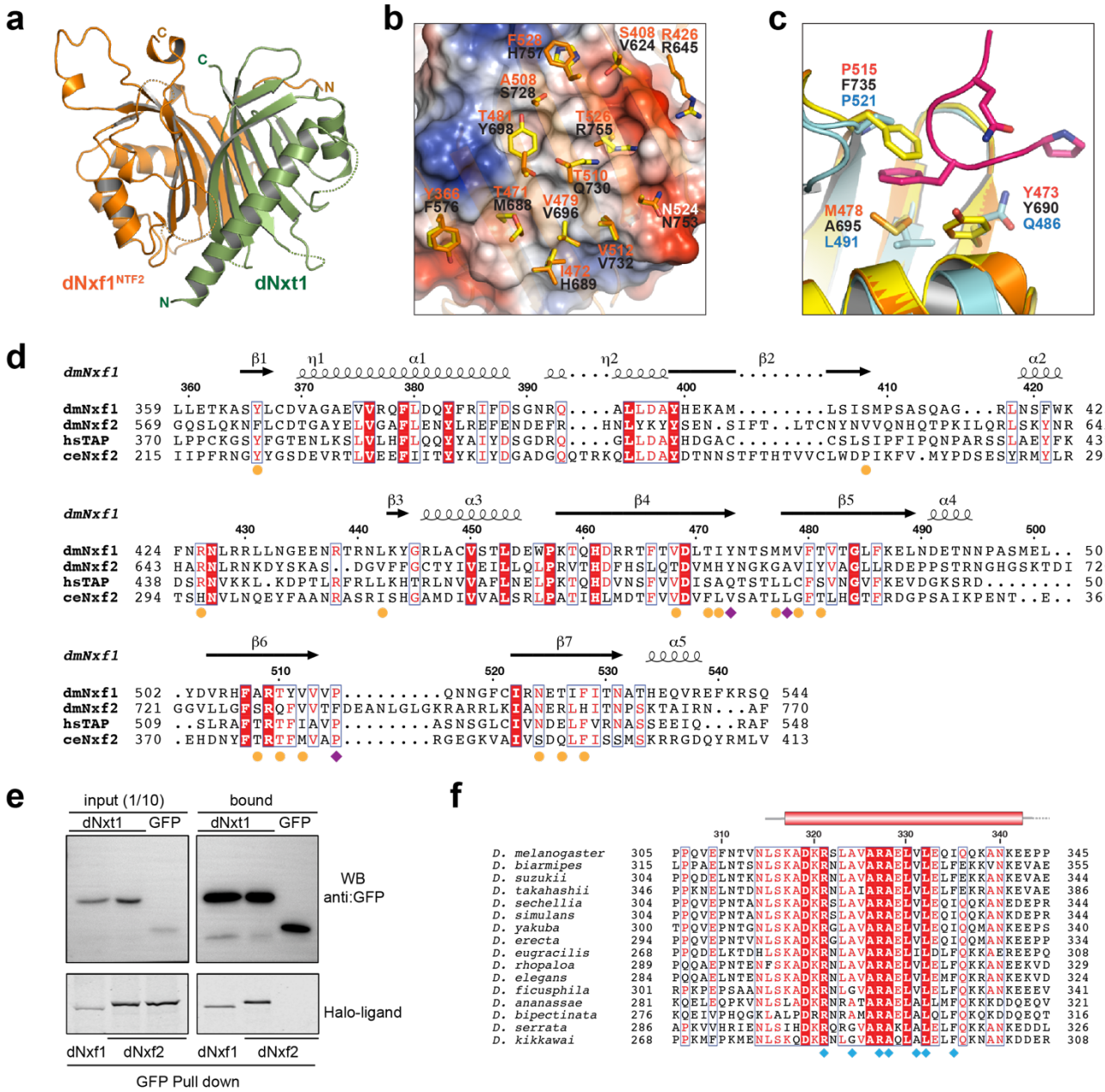

Extended Data Figure 4. dNxf2 Structural analysis of dNxf1^{NTF2} in complex with dNxt1. a, Cartoon representation of dNxf1 NTF2 domain (orange) in complex with dNxt1 (green). **b,** Electrostatic surface potential representation of dNxt1, highlighting hydrophobic and electrostatic surfaces continuously from acidic (red) to non-polar (grey), to basic (blue). Key residues of dNxf1 are shown in stick mode (orange). The corresponding residues in dNxf2 (yellow) are modelled in Coot by mutation operation based on the dNxf1 structure in this study. **c,** dNxf1 NTF2 (orange) and dNxf2 NTF2 (yellow, model based on dNxf1 structure) are superimposed with human TAP NTF2 domain (cyan, PDB accession code 1JN5). Key residues that interact with the Phenylalanine-Glycine (FG) peptide (magenta) are labelled and shown in sticks. **d,** Sequence alignment of the NTF2 domains of dNxf1, dNxf2, human TAP (Q9UBU9), and ceNxf2 (Q9XVS8). The secondary structure annotation of dNxf1 is shown on the top. Residue positions of the reference sequence (dNxf1) are also indicated above the sequences. Arrows and spirals indicate beta-strands and alpha-helices, respectively. Red letters indicate similar residue; white letters in red shading indicate identical residues; blue boxes indicate conserved positions. **e,** Western blots and Halo-ligand staining showing co-immunoprecipitation of GFP-tagged dNxt1 with Halo-tagged dNxf1 or dNxf2 from OSC cells. GFP serves as a negative control. **f,** Sequence alignment of the region of Panx that interacted with dNxf2. Residues involved in the interactions are marked by teal diamond.

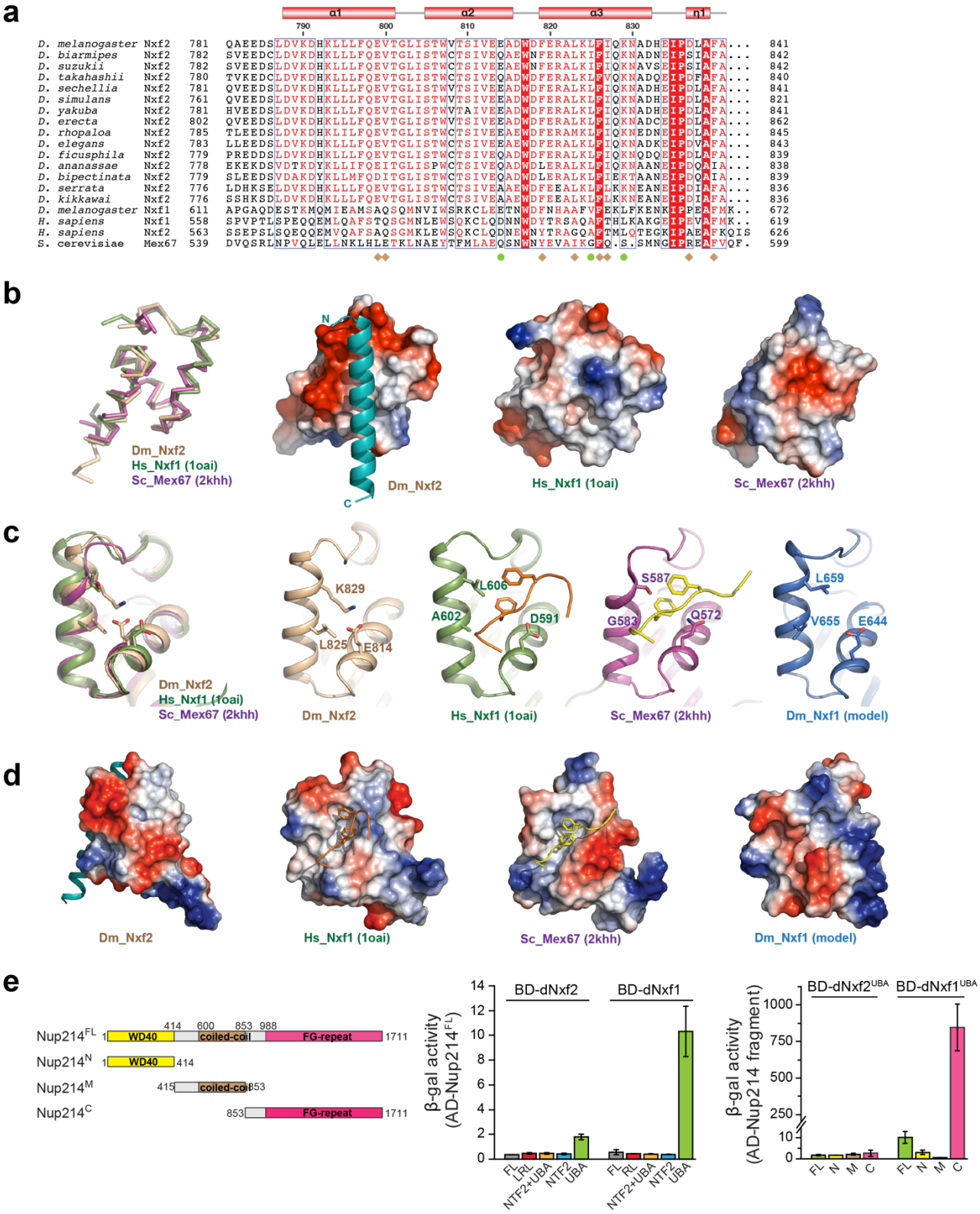

Extended Data Figure 5. Structural comparison of the UBA domains from different NXF family proteins. a, Sequence alignment of the UBA domains of Nxf family proteins. Residues within the dNxf2-Panx interaction interface are indicated in brown diamond. Residues that blocks the entry of the FG peptides are indicated in green circle. Residues that are identical are shown in white with red shading. Residues with high similarities are shown in red. Secondary structural elements are indicated above. **b,** Superimposition of the UBA domains of dNxf2 (wheat), human Nxf1 (green, PDB ID: 1OAI), and yeast Mex67 (purple, PDB ID: 2KHH). Electrostatic potential analysis showing that the corresponding surfaces in the UBA domains of dNxf2 (left), human Nxf1 (middle) and yeast Mex67 (right) are

positively charged and negatively charged, respectively. **Fig. 3c** was shown here again for comparison. **c,** Detailed view, left to right, of the UBA domains of dNxf2, human TAP, yeast Mex67, and dNxf1 (model). The dNxf1 model was generated by SWISS-MODEL server. In human Nxf1 and yeast Mex67, the FG peptides bind in the concave passage formed by α2 and α3. **d,** Electrostatic potential analysis showing a closed surface on dNxf2 UBA that blocks the entry of FG-nup. In the corresponding surface of dNxf2 UBA, the passage for the peptide is blocked (left). Human Nxf1 UBA (PDB ID: 1OAI) and yeast Mex67 UBA (PDB ID: 2KHH) show a hydrophobic pocket to accommodate the two phenylalanines of the FxFG peptides (middle). A model of dNxf1 UBA (right) indicates that a peptide binding pocket may exist on the dNxf1 surface. **e,** Y2H assays show that dNxf1 UBA domain but not dNxf2 UBA interacts with Nup214 FG-repeat region. Interactions were determined by either measuring the beta-galactosidase activity produced by the reporter gene. Data are averages of three independent experiments (n=3). Proteins or fragments of Nup214 are shown above the dashed line.

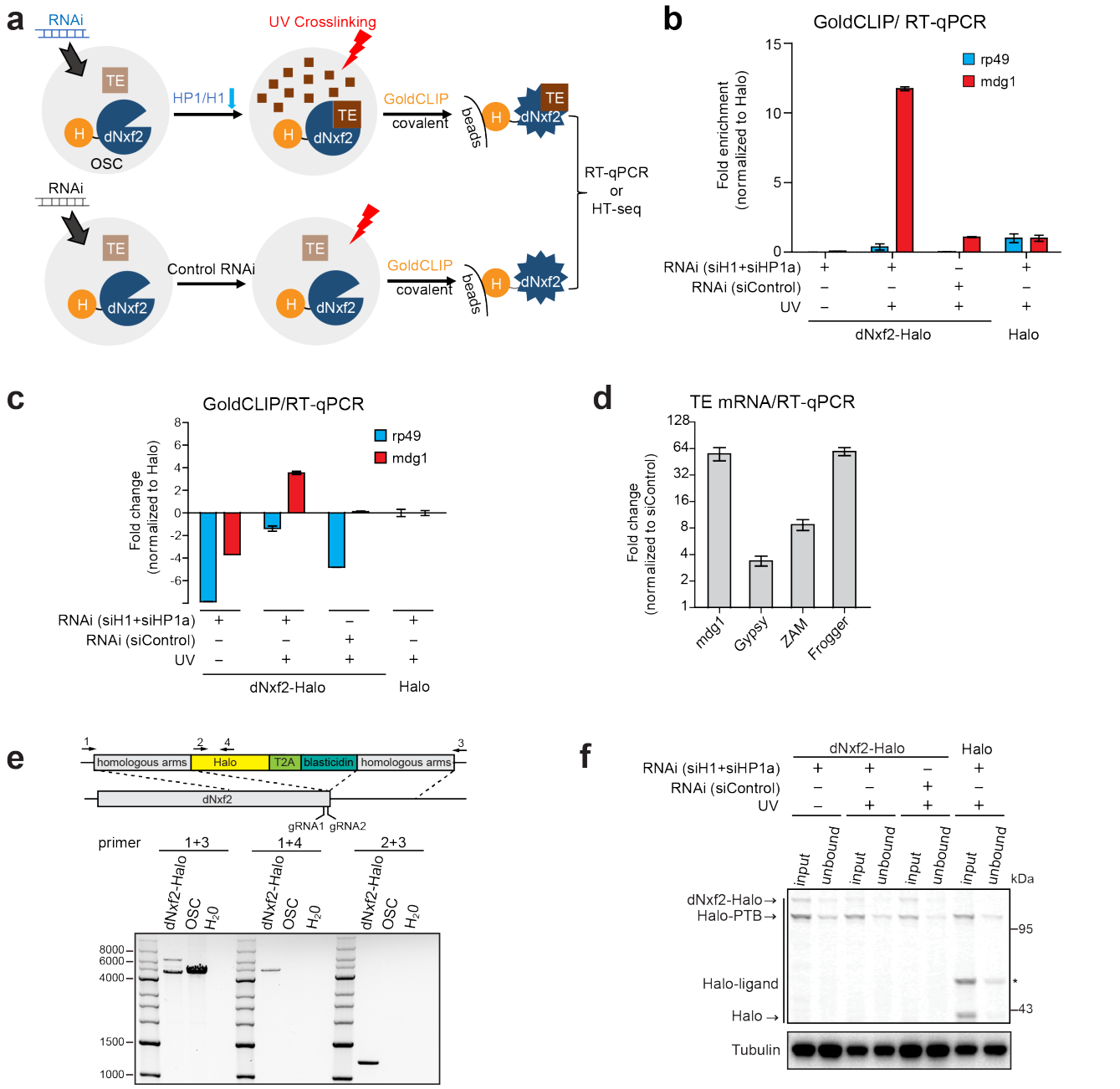

Extended Data Figure 6. dNxf2 specifically binds to transposons *in vivo*. a, Schematic representation of the GoldCLIP experiments. OSC, Ovarian Somatic Cell. TE, transposon. H, Halo-tag. **b,** RT-qPCR results showing relative levels of the mdg1 transposon or rp49 for dNxf2-Halo GoldCLIP sample, compared to either no UV or a Halo control**.** Fold enrichments are calculated as a mammalian spike-in normalized RNA levels divided by that of the input samples. For comparison, the value of Halo control was used for normalization. Mean values ± s.d. from 3 independent experiments are shown. **c,** Data from **b** was redrawn in $\log_2$ scale showing relative enrichment or depletion of the indicated transcripts, normalized to the Halo alone control. **d,** RT-qPCR results showing relative steady-state RNA levels of the indicated transposons for OSC from the H1+HP1a double siRNA knockdown, compared to a control siRNA knockdown. Fold changes are calculated as *rp49*-normalized RNA levels divided by that of the corresponding controls. Mean values ± s.d. from 3 independent experiments are shown. **e,** A Schematic of the knock-in strategy is displayed. Agarose gel showing PCR results confirming a correct integration of Halo-tag to the C-terminus of the dNxf2 locus. PCR primers amplifying the indicated regions are shown on the top and two sgRNAs targeting near the stop codon of dNxf2 are indicated at the bottom of the schematic. **f,** Western blots and Halo-ligand staining showing depletion of dNxf2-Halo or Halo alone by Halo pull down. Beta-tubulin blots serve as a loading control. The asterix indicates non-specific bands stained by Halo-ligand.

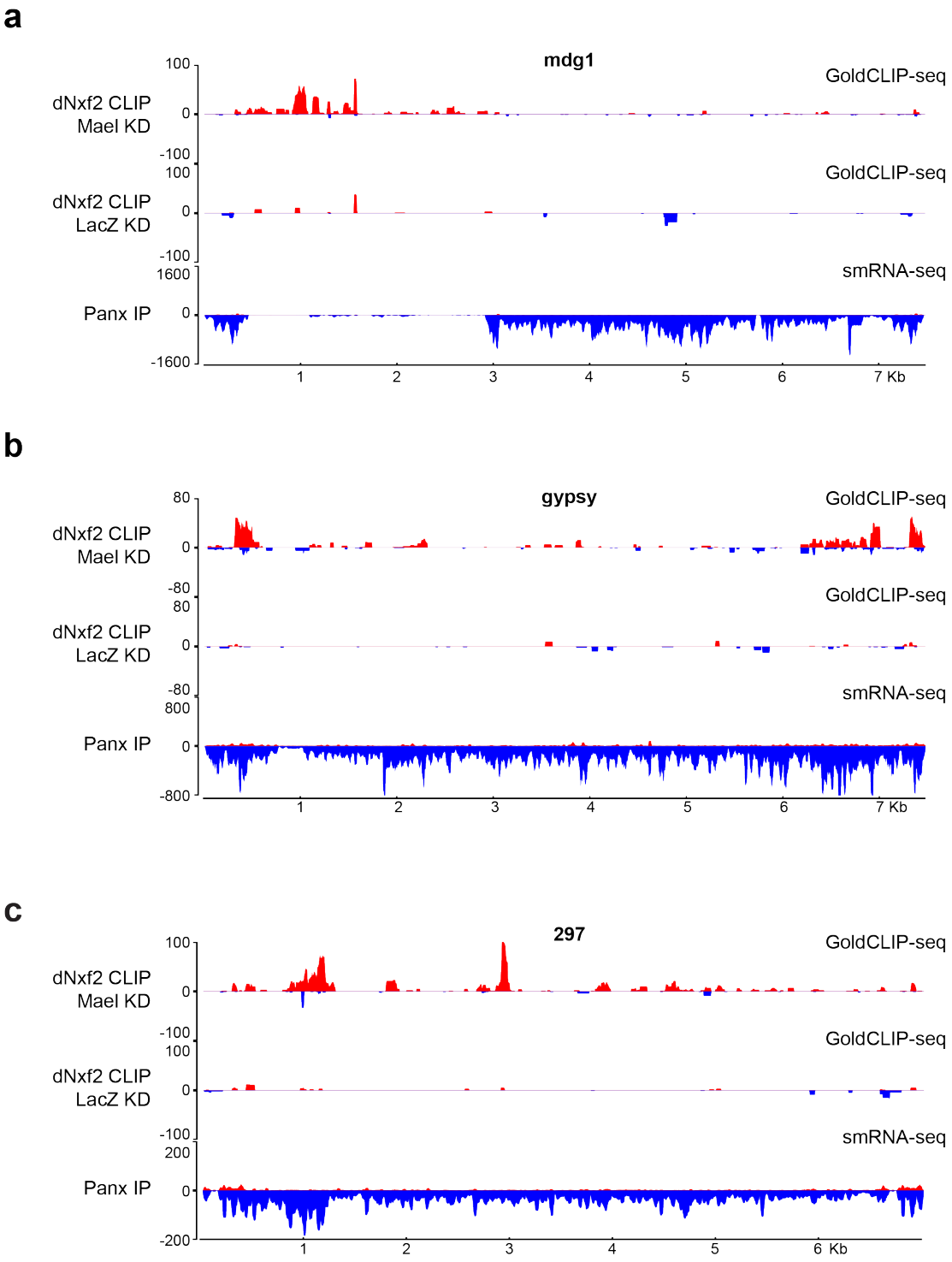

435
436 **Extended Data Figure 7. dNxf2 binds to Piwi/piRNA targeted transposons**. **a,** Density plots for dNxf2-Halo
437 GoldCLIP reads from Mael knockdown OSCs (top panel), dNxf2-Halo GoldCLIP reads from LacZ knockdown OSCs
438 (middle panel), and Panx co-immunoprecipitated smRNA reads (bottom panel, from previously published data[20]) over
439 the transposon consensus of mdg1. **b** and **c** are the same as in **a** except for gypsy (**b**) and 297 (**c**).
440

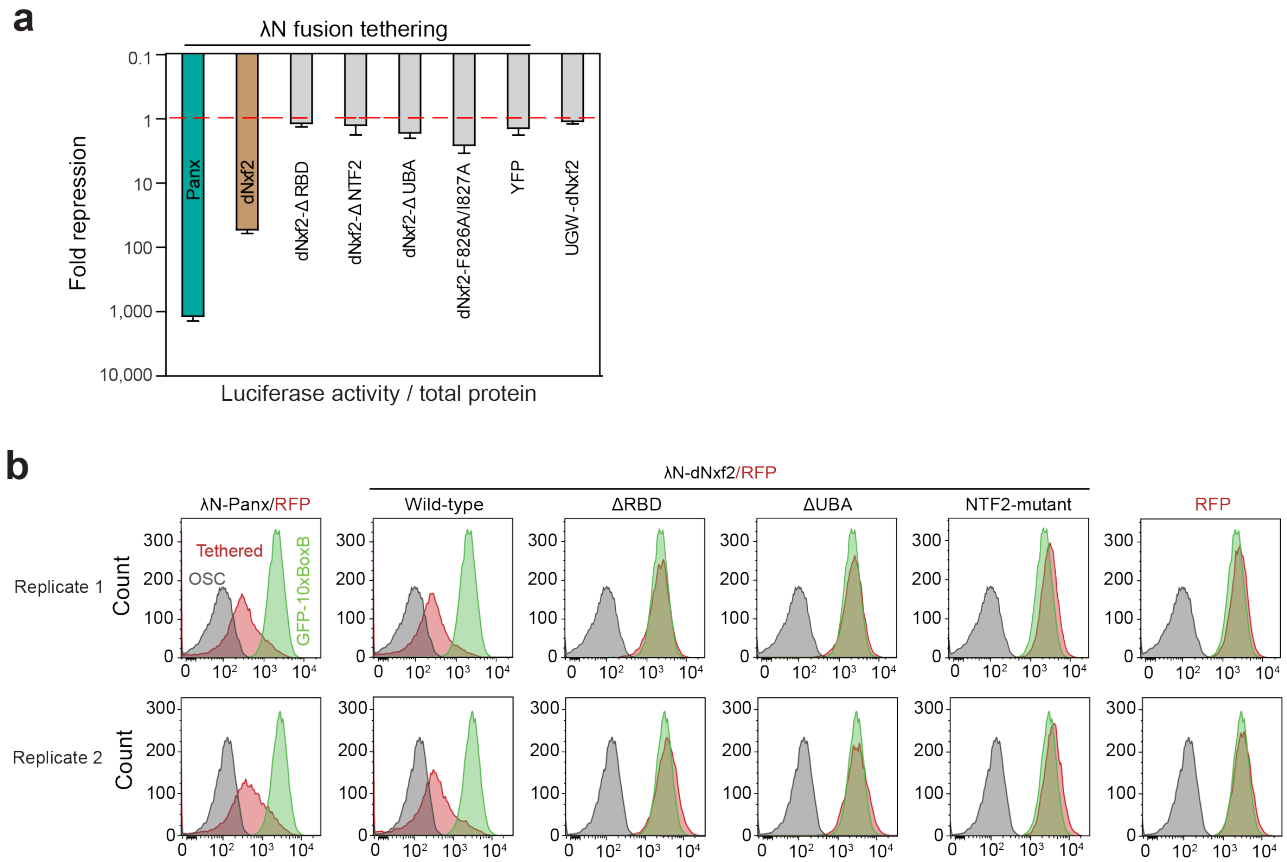

Extended Data Figure 8. The Pandas complex is required for piRNA-guided transposon silencing. a, Effects of the indicated λN fusion proteins or a non-tethering control (GFP-dNxf2) on luciferase activity of the reporters integrated into the attP2 landing site. Data from **Fig. 3g** was shown here again for comparison. Data show mean ± s.d. (n = 15). **b,** FACS sorting showing counts and fluorescence of GFP positive cells gated by high RFP expressing OSCs electro-transfected with the indicated plasmids expressing different λN-fusion proteins. OSC (grey), autofluorescence of OSCs without any GFP reporter; Tethered (red), GFP reporter OSCs transfected with the indicated expression plasmids; GFP-10xBoxB (green), GFP reporter cells with no transfection.

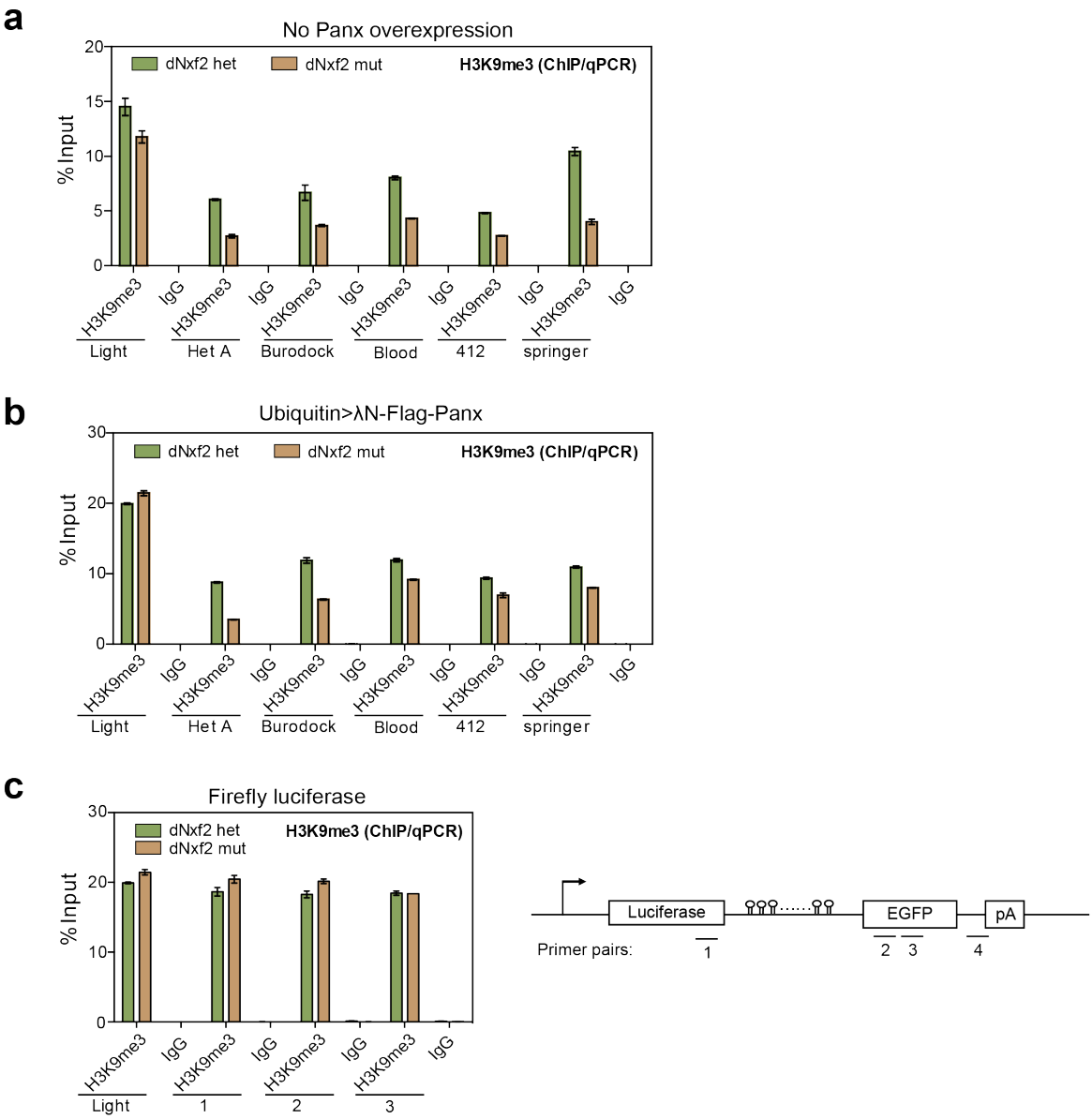

Extended Data Figure 9. ChIP-qPCR assays measuring H3K9me3 changes upon loss of dNxf2. a, H3K9me3 mark enrichments at transposons comparing heterozygous and mutant for dNxf2. **b,** H3K9me3 mark enrichments at the indicated transposons comparing heterozygous and mutant for dNxf2 when overexpressing Panx driven by a Ubiquitin promoter. Green and brown bar, polyclonal antibody specific to H3K9me3; Black and grey bar, pre-immune rabbit IgG. Mean values ± s.d. from 3 independent experiments are shown. **c,** H3K9me3 mark enrichments at the Firefly-10xBoxB reporter tethered with λN-flag-Panx in the same genetic background as in **b**. Schematic of qPCR primer pair positions is shown on the right.

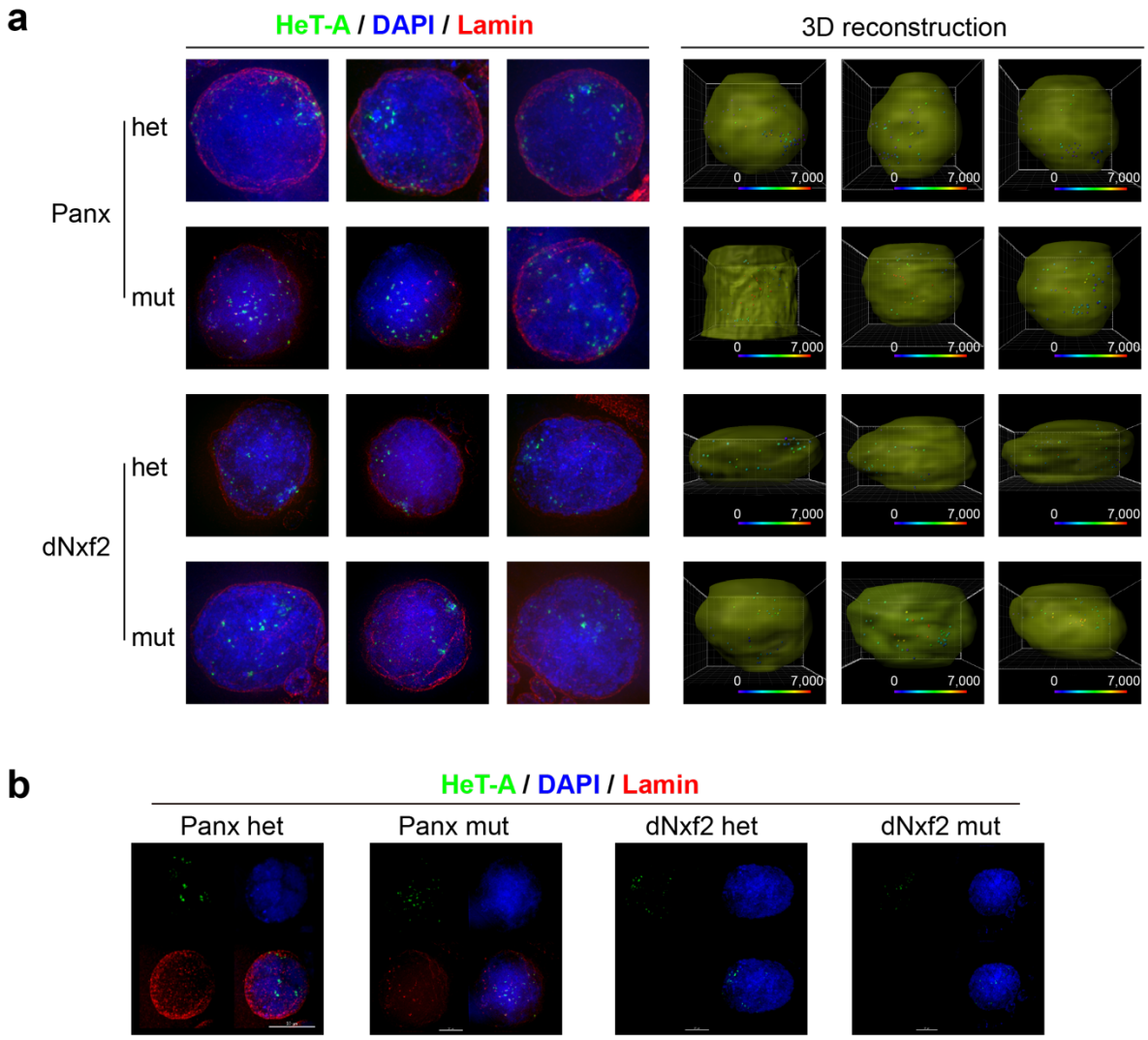

Extended Data Figure 10. Het-A left nuclear peripheries upon loss of either Panx or dNxf2. a, Left three columns showing 3D SIM super-resolution microscopy of DNA FISH (HeT-A, green) and Lamin A (red) double staining from either Panx or dNxf2 heterozygote versus mutant ovaries. Right three columns, estimation of the positioning of clustered HeT-A signals relative to the nuclear membrane of nurse cells. 10-20 nuclei were quantified for each condition. The distance was displayed in a blue-red scale with red indicating longer distance between the green dots and nuclear membrane. **b,** Projections of the 3D videos on the *XY* surface either in combination (bottom right) or in split channels for DAPI (blue, upper right), Lamin (red, bottom left) and HeT-A (green, upper left) on the selected ovaries from **a**. See also Supplementary Movies 1-4.

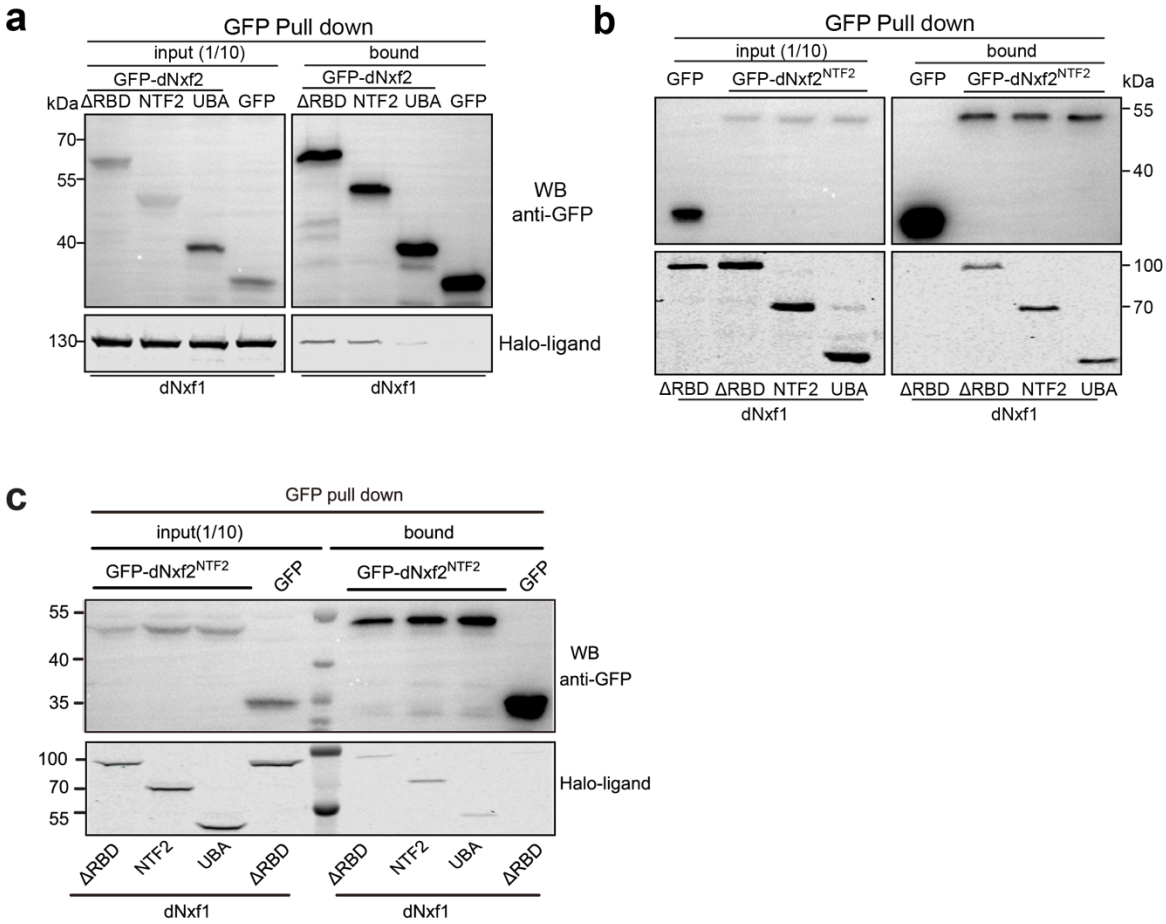

Extended Data Figure 11. dNxf2 interacts with dNxf1 in *Drosophila* cell lines. a, Western blots and Halo-ligand staining showing co-immunoprecipitation of GFP-tagged various truncated dNxf2 with Halo-tagged full length dNxf1 from OSC cells. ΔRBD, dNxf2 lacking N-terminus RNA binding domains; NTF2, dNxf2^{NTF2} domain; UBA, dNxf2^{UBA} domain. **b,** Western blots and Halo-ligand staining showing co-immunoprecipitation of GFP-tagged dNxf1^{NTF2} domain with Halo-tagged various truncated dNxf1 from S2 cells. ΔRBD, dNxf1 lacking all N-terminus RNA binding domains; NTF2, dNxf1^{NTF2} domain; UBA, dNxf1^{UBA} domain. GFP serves as a negative control. **c,** The same as in B except the experiments were done using OSC cells.

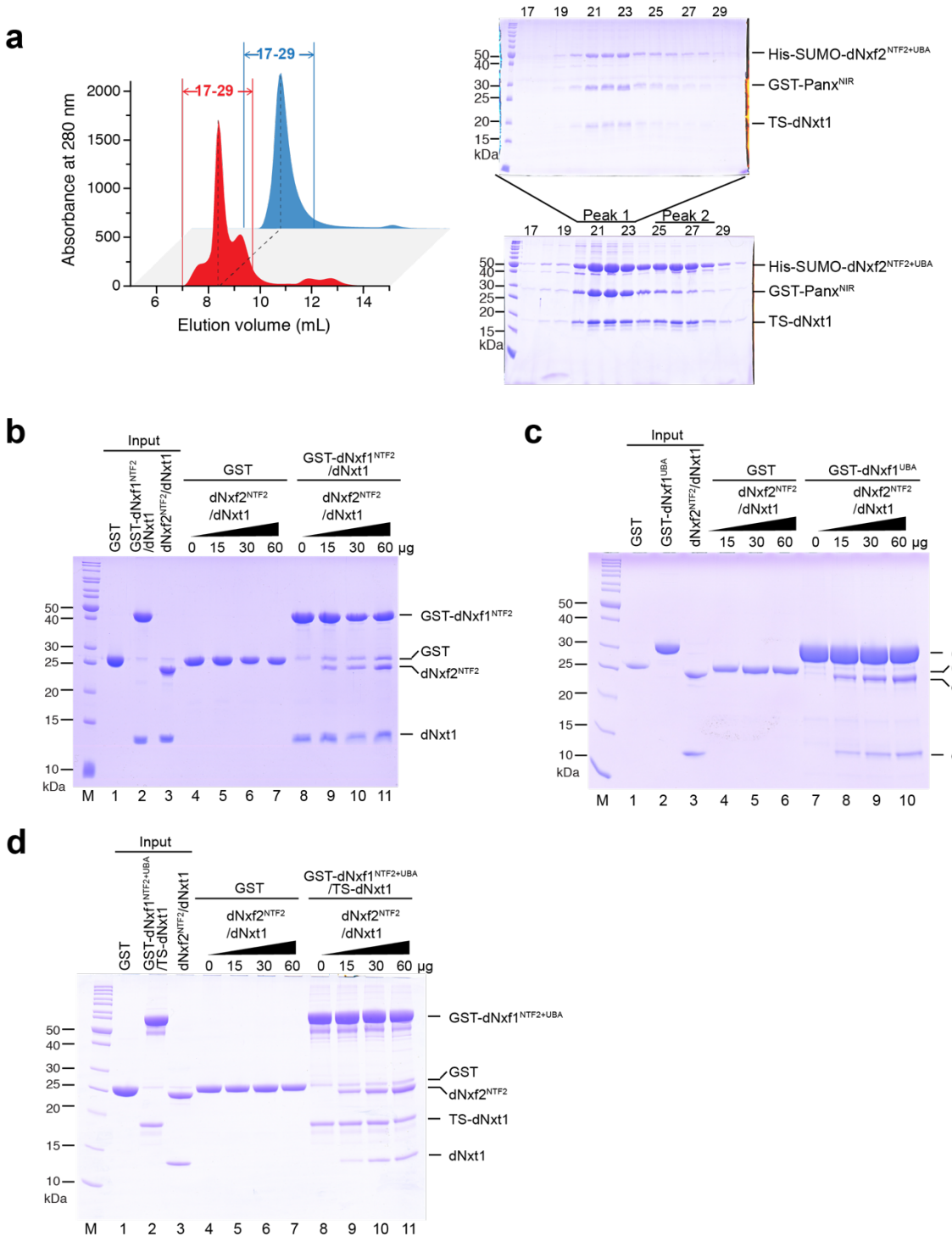

Extended Data Figure 12. dNxf1 directly interacts with the NTF2 domain of dNxf2 via either NTF2 or UBA domains. a, dNxf2$^{NTF2+UBA}$, dNxt1, and Panx^{NIR} form a ternary complex in solution as shown on the size exclusion chromatography profile. Left panel, OD280 trace; Right panel, SDS-PAGE shows the components of the peak in the elution profile. **b-d,** GST pull-down assays showed the direct interactions between dNxf1 and dNxf2. Each of 60 µg of purified GST-dNxf1^{NTF2}/dNxt1 (**b**), GST-dNxf1^{UBA} (**c**), GST-dNxf1$^{NTF2+UBA}$/TS-dNxt1 complex (**d**) and GST protein was immobilized on GSH beads, respectively. Increasing amounts of dNxf2^{NTF2}/dNxt1 complex (0, 15, 30, 60 µg) were added and incubated. The beads were washed and aliquots of the bound fractions (8%) were analyzed by SDS-PAGE. Each input protein of 2 µg was loaded on SDS-PAGE as well. Positions of molecular weight markers are indicated on the left in kDa.

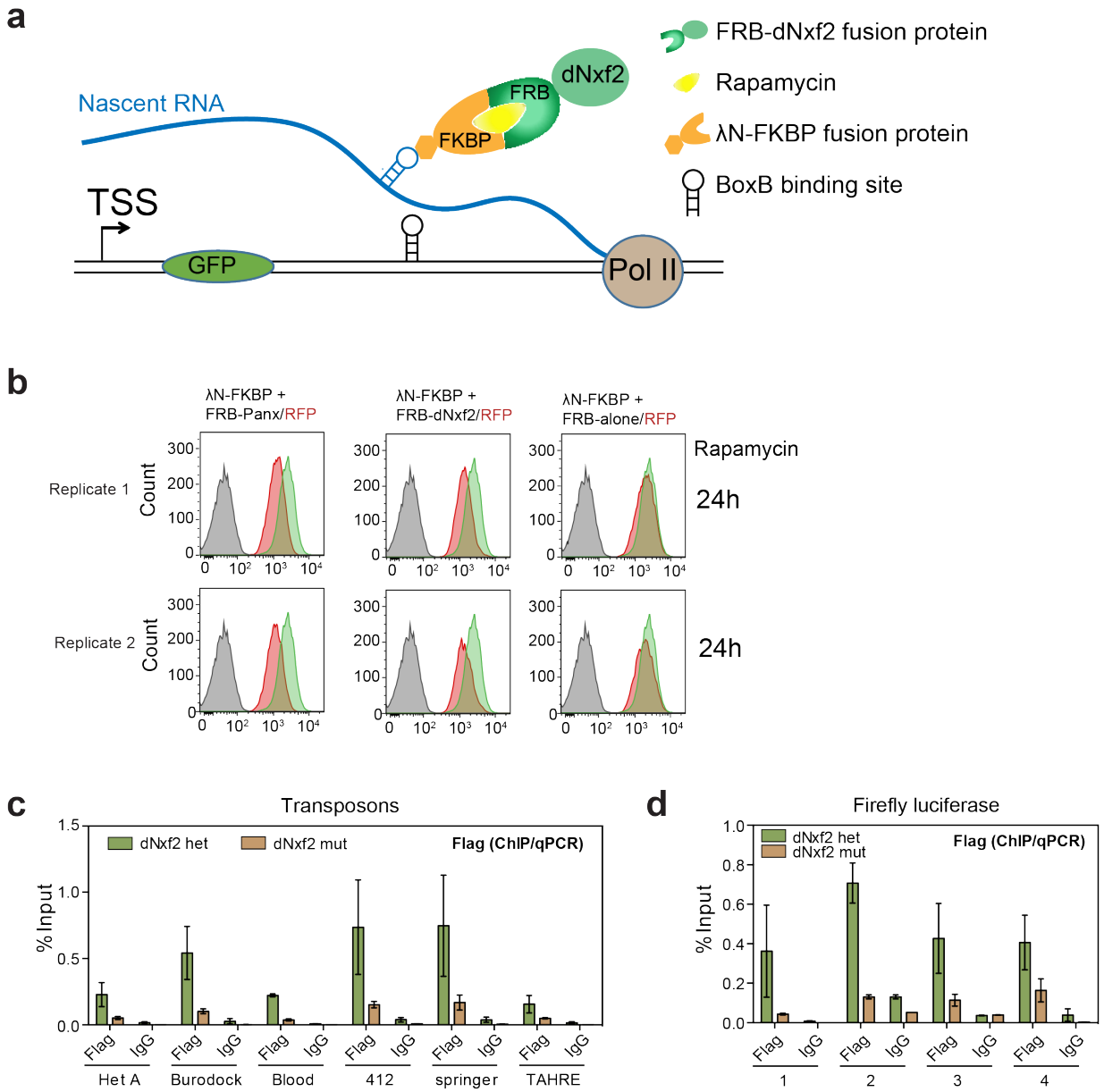

Extended Data Figure 13. Rapamycin inducible tethering system. a, Schematic representation of a rapamycin-inducible system for λN-FKBP:FRB tethering. **b,** FACS sorting showing counts and fluorescence of GFP positive cells gated by high RFP expressing OSCs (as in **Extended Data Fig. 7b**) transfected with the plasmids expressing both λN-FKBP and the indicated FRB-fusion proteins. 24 hours after transfection, cells were treated with rapamycin for additional 24 hours. Two independent biological replicates were shown. **c,** Flag-Panx enrichments at the indicated transposons comparing heterozygous and mutant for dNxf2 when overexpressing Panx driven by a Ubiquitin promoter. Green and brown bar, monoclone antibody specific to Flag (M2); Black and grey bar, pre-immune mouse IgG. Mean values ± s.d. from 3 independent experiments are shown. **d,** Flag-Panx enrichments at the Firefly-10xBoxB reporter tethered with λN-flag-Panx in the same genetic background as in (**c**). Schematic of qPCR primer pair positions is shown in **Extended Data Fig. 9c**.

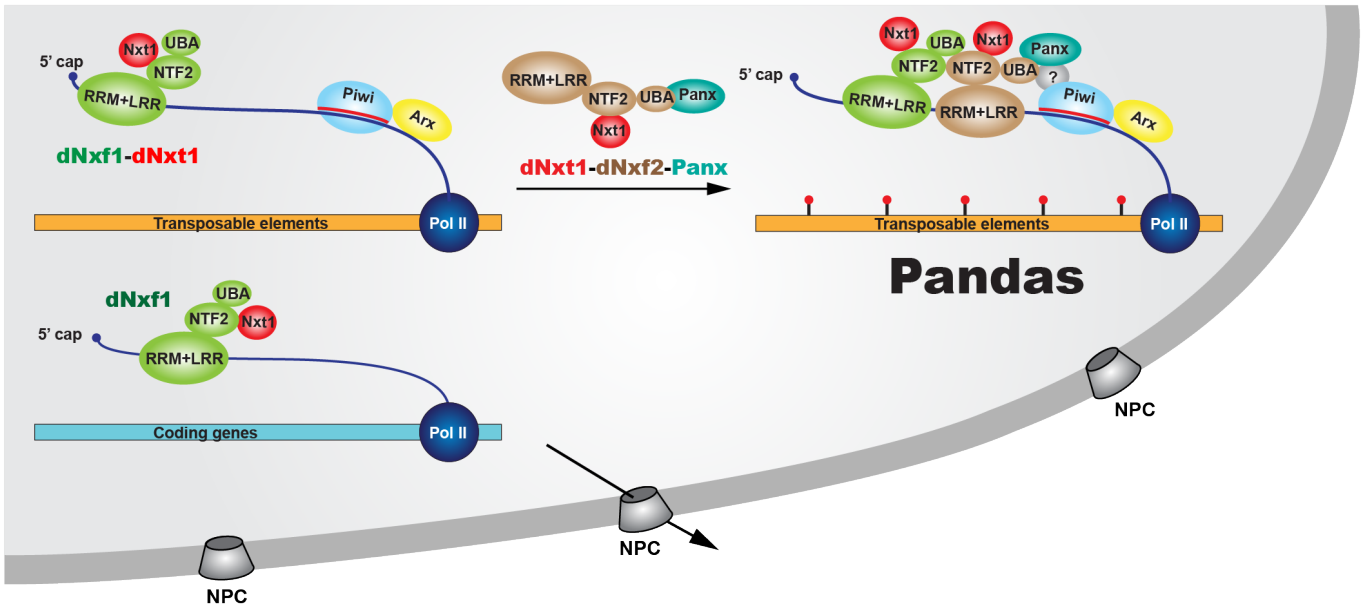

Extended Data Figure 14. A model for the Pandas (Panoramix-dNxf2 dependent TAP/p15 silencing) complex in piRNA-guided silencing, preventing transposon RNA export when targeted by Piwi:piRNAs.